MOLECULAR AND CELLULAR BIOLOGY, June 2005, p. 5253–5269 Vol. 25, No. 12
0270-7306/05/$08.00+0 doi:10.1128/MCB.25.12.5253–5269.2005

Rab3D Regulates a Novel Vesicular Trafficking Pathway That Is Required for Osteoclastic Bone Resorption†

Nathan J. Pavlos,[1] Jiake Xu,[1] Dietmar Riedel,[3] Joyce S. G. Yeoh,[1]‡ Steven L. Teitelbaum,[4] John M. Papadimitriou,[2] Reinhard Jahn,[3] F. Patrick Ross,[4]* and Ming H. Zheng[1]*

Units of Orthopaedics[1] and Pathology,[2] School of Surgery and Pathology, University of Western Australia, QEII Medical Centre, Perth, Western Australia, Australia; Department of Neurobiology, Max Planck Institute for Biophysical Chemistry, Göttingen 37077, Germany[3]; and Department of Pathology, Washington University School of Medicine, St. Louis, Missouri[4]

Received 6 December 2004/Returned for modification 10 February 2005/Accepted 4 March 2005

Rab3 proteins are a subfamily of GTPases, known to mediate membrane transport in eukaryotic cells and play a role in exocytosis. Our data indicate that Rab3D is the major Rab3 species expressed in osteoclasts. To investigate the role of Rab3D in osteoclast physiology we examined the skeletal architecture of Rab3D-deficient mice and found an osteosclerotic phenotype. Although basal osteoclast number in null animals is normal the total eroded surface is significantly reduced, suggesting that the resorptive defect is due to attenuated osteoclast activity. Consistent with this hypothesis, ultrastructural analysis reveals that Rab3D$^{-/-}$ osteoclasts exhibit irregular ruffled borders. Furthermore, while overexpression of wild-type, constitutively active, or prenylation-deficient Rab3D has no significant effects, overexpression of GTP-binding-deficient Rab3D impairs bone resorption in vitro. Finally, subcellular localization studies reveal that, unlike wild-type or constitutively active Rab3D, which associate with a nonendosomal/lysosomal subset of post-*trans*-Golgi network (TGN) vesicles, inactive Rab3D localizes to the TGN and inhibits biogenesis of Rab3D-bearing vesicles. Collectively, our data suggest that Rab3D modulates a post-TGN trafficking step that is required for osteoclastic bone resorption.

Osteoclasts (OCs) are bone-resorbing polarized polykaryons derived from cells of the myeloid lineage, (70) whose activity is obligatory for skeletal maturation, tooth eruption and the maintenance of calcium homeostasis (71, 74). Following attachment to bone, OCs undergo plasmalemmal and cytoskeletal reorganization, resulting in formation of a highly enfolded and specialized membrane domain, known as the ruffled border, that acts as the resorptive organelle of these cells. As a consequence, both protons and a number of bone resorbing enzymes, such as cathepsin K, type IV collagenase and other matrix metalloproteinases (MMPs) are released into the underlying resorption lacuna (68). In addition to its exocytic properties, the ruffled border facilitates removal of degraded bone matrix products via transcytosis (47, 48, 61, 69). Thus, like other polarized cells, OCs require an intricate balance between exocytic and endocytic vesicular trafficking to preserve ruffled border membrane asymmetry and sustain their unique structural and functional segregation during bone resorption. At present little is known about the molecular machinery that regulates these transport pathways in OCs, although they are predicted to share basic mechanism(s) with other vesicular fusion systems conserved from yeast to neurons (46).

Current models of membrane fusion are dominated by consideration of two types of proteins, namely small G proteins of the Rab family and soluble *N*-ethylmaleimide-sensitive attachment protein receptors (SNAREs) (31). Whereas SNAREs and their interacting proteins play crucial roles in lipid bilayer fusion, members of the Rab GTPase superfamily have emerged as key regulators of vesicular budding, motility, tethering and docking at all stages of exocytic and endocytic transport (57, 80). Over 60 Rabs exist in mammalian cells, each displaying differential expression and subcellular localization (56). Like other regulatory GTPases, Rabs act as molecular switches, cycling between GTP-bound (activated) and GDP-bound (inactive) conformations, enabling Rabs to recruit specific downstream effector protein complexes through which they elicit their biological functions (80).

The Rab3 proteins (Rab3A, -B, -C, -D) are a highly homologous subfamily of Rabs thought to play important roles in regulated exocytosis (32). Unlike most Rabs which are ubiquitously expressed, the different Rab3 members are restricted to cells types with high exocytic requirements (38, 45). Thus, Rab3A and C are expressed predominantly in neurons and neuroendocrine cells where they both localize to synaptic vesicles and secretory granules (22, 23). Rab3B is associated with tight junctions and secretory granules in epithelial cells and anterior pituitary glands (39, 78). In contrast, Rab3D is widely expressed in nonneuronal cells including adipocytes, exocrine glands and several haematopoietic cells, where it localizes to secretory granules and vesicles (4, 50, 58, 76). Accumulated evidence suggests that Rab3A and Rab3C act as negative regulators of exocytosis (25, 28), whereas Rab3B and Rab3D are positive modulators of the same process (5, 15, 39, 53, 60).

* Corresponding author. Mailing address for Ming H. Zheng: Unit of Orthopaedics, School of Surgery and Pathology, University of Western Australia, 2nd Floor "M" Block, QEII Medical Centre, Nedlands, Perth, Western Australia 6009, Australia. Phone: 61 (8) 9346-4050. Fax: 61 (8) 9346-3210. E-mail: zheng@cyllene.uwa.edu.au. Mailing address for F. Patrick Ross: Department of Pathology and Immunology, Washington University School of Medicine, Campus Box 8118, 660 South Euclid Avenue, St. Louis, MO 63110. Phone: (314) 454-8079. Fax: (314) 454-5505. E-mail:rossf@wustl.edu.

† Supplemental material for this article may be found at http://mcb.asm.org/.

‡ Present address: Department of Stem Cell Biology, University of Groningen, University Hospital Groningen, A. Deusinglaan 1, NL-9713 AV Groningen, The Netherlands.

TABLE 1. Degenerate and isoform-specific primers for mouse Rab3 cDNAs[a]

Region	Sense primer	Antisense primer
mRab3 deg.	5′ CARAAYTTYGAYTAYATG 3′ (D1)	5′ NACYTGNGCRTTRTCCCA 3′ (D2)
mRab3A	5′ ATGGCTTCCGCCACAGACTC 3′	5′ TCAGCAGGCACAATCCTGAT 3′
mRab3B	5′ ATGGCTTCAGTGACTGAT 3′	5′ CTAACAAGAGCAGTTCTG 3′
mRab3C	5′ GGAATTCACAATGAGACACGAGGCG 3′	5′ GCTCTAGAGCTTAGCCAGCCACAGTTGGG 3′
mRab3D	5′ ATGGCATCCGCTAGTGAG 3′	5′ CTAACAGCTGCAGCTGCT 3′
mTRAP	5′ TGTGGCCATCTTTATGCT 3′	5′ GTCATTTCTTTGGGGCTT 3′
mCTR	5′ TGGTTGAGGTTGTGCCCA 3′	5′ CTCGTGGGTTTGCCTCATC 3′
mCATH K	5′ GGGAGAAAAACCTGAAGC 3′	5′ ATTCTGGGGACTCAGAGC 3′
m36B4	5′ TCATTGTGGGAGCAGACA 3′	5′ TCCTCCGACTCTTCCTTT 3′

[a] Primer sequences were derived based on the published sequences deposited in GenBank.

In the present study, we report the existence of Rab3D as the major isoform in mouse OCs and their precursors. Disruption of Rab3D function by either targeted inactivation or overexpression of a dominant-inhibitory Rab3D mutant impairs osteoclastic bone resorption in vivo and in vitro, respectively. Interestingly, this disruption correlates with morphological disturbances in the ruffled border membrane. Localization studies reveal that wild-type Rab3D associates with a subset of post-*trans*-Golgi network (post-TGN) vesicles reminiscent of secretory granules, while expression of dominant inhibitory Rab3DN135I inhibits the biogenesis of these compartments. Our data suggest that Rab3D is involved in regulating a previously uncharacterized post-TGN vesicle trafficking step that contributes to the maintenance of the OC ruffled border membrane and hence modulates the major function of the cell, namely bone resorption.

MATERIALS AND METHODS

Antibodies and reagents. A primary rabbit polyclonal Living Colors A.v. Peptide anti-enhanced green fluorescent protein (anti-EGFP) antibody was purchased from Clontech Laboratories Inc, Palo Alto, CA. A rabbit polyclonal anti-mouse Rab3A (K-15) antibody was purchased from Santa Cruz Biotechnology Inc., Santa Cruz, CA. Rabbit polyclonal anti-mouse Rab3 (Cl42.1) antibody was obtained from Synaptic Systems, Göttingen, Germany. The generation and characterization of polyclonal rabbit anti-Rab3D antibodies used in this study have been described previously (58, 59). Rabbit polyclonal anti-rat TGN38 raised against the C-terminal was kindly donated by George Banting (40). Alexa Fluor 546-conjugated goat anti-mouse immunoglobulin G (IgG), goat anti-rabbit IgG, rhodamine-conjugated Phalloidin and Hoechst dye were all purchased from Molecular Probes Inc., Eugene, OR. Triton X-114 was purchased from Sigma, St. Louis, MO, while horseradish peroxidase (HRP)-conjugated goat anti-mouse IgG and enhanced chemiluminescence (ECL) detection kits were purchased from Amersham Life Science, Buckinghamshire, United Kingdom. RAW 264.7 murine macrophage/monocytes (clone C4) were kindly provided by Ian Cassady (12). All tissue culture reagents were purchased from GIBCO-BRL, Life Technologies, Melbourne, Australia, unless stated otherwise.

Generation and isolation of mouse osteoclasts. OCs were generated in vitro using one of two culture systems. First, RAW 264.7 cells were cultured in T-25 culture flasks at 10^5 cells/flask, in six-well plates at 2×10^4 to 2.5×10^4 cells/well, in 96-well plates at 1×10^3 to 1.5×10^3 cells/well or on glass coverslips in 24-well plates at 10^4 cells/well in minimal essential medium alpha modification (α-MEM) containing recombinant glutathione *S*-transferase (GST)–RANK ligand (RANKL) (37, 79) at 50 to 100 ng/ml, with replacement of culture media every 2 to 3 days. OCs were evident after 5 to 7 days of culture. Cells were subsequently harvested and processed for total RNA extraction, immunoblotting, or immunocytochemistry. Alternatively, OCs were prepared from bone marrow macrophages (BMMs) by culture in α-MEM–10% fetal bovine serum (FBS) at a starting density of 1.5×10^5 cells per well in 48 well plates in the presence of 50 ng/ml human recombinant macrophage colony-stimulating factor (M-CSF; R&D Systems, Minneapolis, MN). After 3 days, cells were cultured for a further 4 days with GST-RANKL (100 ng/ml) and M-CSF (20 ng/ml). Cells were fixed and stained for the OC marker tartrate-resistant acid phosphatase (TRAP). OCs were scored as TRAP+ multinucleated (more than three nuclei) cells. Cells were subsequently harvested and processed for total RNA extraction, Western blot analysis, or immunofluorescence confocal microscopy.

Mature primary OCs were mechanically disaggregated from the long bones of 1- to 3-day-old mice essentially as described in detail by the methods of Boyde et al. (8) and Chambers et al. (13). Isolated cells were seeded onto either glass or dentin surfaces for 24 h before being fixed and processed for immunohistochemistry.

Tartrate-resistant acid phosphatase staining and bone resorption pit assay. Cells were stained for TRAP using a commercially available kit (387-A; Sigma), according to published methods (37). After staining, cells were rinsed with phosphate-buffered saline (PBS) and photographed and quantified under a light microscope. To study the ability of OCs to form resorption pits on dentin, RAW 264.7 cells and BMMs were seeded onto 150-μm-thick dentin slices and cultured for 9 days in the presence of either GST-RANKL alone or in combination with M-CSF. After 9 days, OCs were fixed and stained for TRAP activity. Dentin slices were then incubated in 2 M NaOH (2 h) and cells were removed by mechanical agitation and sonication. Resorption lacunae were visualized by scanning electron microscopy (SEM) (82) and resorptive parameters quantitated using Scion Image software (Scion Corporation, National Institutes of Health).

Reverse transcription (RT)-PCR cloning, Southern blotting, and sequence analysis. Mouse OC and brain cDNAs served as templates for the identification and isolation of Rab3 genes. Rab3 degenerative oligonucleotide primers were designed based on the conserved sequences of Rab3/Ras consensus amino acid sequences D1 (QNFDYM) and D2 (WDNAQV) (Genset Pacific Pty. Ltd., Lismore, Australia) (Table 1.). Total RNA was extracted from either mouse bone marrow-derived OCs or snap frozen adult mouse brain (C57 black) with RNAzol B (Tel Test, Friendswood, Texas) and mRNA was enriched using DYNABEADS in accordance to the manufacturer's instructions (DYNAL Inc., Lake Success, NY). cDNAs were synthesized from 2 μg of purified mRNA using 100 U of Moloney murine leukemia virus (M-MLV) reverse transcriptase (Promega Corp., Madison, WI) as described by the manufacturer's guidelines. PCR was performed using 1.0 U DyNAzyme polymerase (GeneWorks, Hindmarsh, Australia) with 0.4 mmol/liter of D1 and D2 primers, 125 μmol/liter of dinucleoside triphosphate (dNTP) in 10× PCR buffer (GeneWorks) and water in a total volume of 25 μl. Amplification was performed in a DNA thermal cycler (model 2400; Perkin Elmer, Boston, MA), using 94°C for 5 min, 94°C for 30 s, 50°C for 2 min, 72°C for 30 s, and final extension at 72°C for 10 min. PCR products were electrophoresed on a 1.5% agarose gel containing ethidium bromide (EtBr). A 342-bp amplimer corresponding to the predicted size of Rab3 proteins was gel purified (GeneWorks) and subcloned into a pCR2.1 TA cloning vector (Invitrogen, Mt. Waverly, Australia). A total of 20 clones were sequenced in both directions using an automated ABI 373 system and BLAST N (3) at the National Center for Biotechnology Information (NCBI) was used to screen for DNA and protein homologies via the world wide web.

For Southern blot analysis, agarose gels were depurinated in 0.25 M HCl for 10 min and subsequently transferred by capillary to a Hybond N+ membrane (Amersham Life Science). Following transfer, membranes were washed and hybridized for 16 h at 65°C with an α-P^{32}-labeled mouse Rab3 cDNA probe. Stringency washes were carried out twice with 2× SSC (1× SSC is 0.15 M NaCl plus 0.015 M sodium citrate), 0.1% sodium dodecyl sulfate (SDS) and once with 1× SSC, 0.1% SDS, and 0.2× SSC, 0.1% SDS. Finally membranes were exposed to X-Omat Blue XB-1 X-ray film (Amersham Life Sciences).

Expression of mouse calcitonin receptor (CTR), Cathepsin K (Cath K), TRAP and Rab3 isoforms in RAW 264.7 and RANKL-differentiated OCs was evaluated by RT-PCR amplification using sets of gene specific primers based on published

mouse sequences (Table 1.), using reverse transcription of total RNA isolated with RNAzol B with 100 U of M-MLV reverse transcriptase (Promega). Two microlitres of each cDNA was subjected to PCR using 1.0 U of DyNAzyme polymerase (GeneWorks) with 0.4 mmol/liter of murine CTR, Cath K, TRAP, Rab3A, Rab3B, Rab3C or Rab3D specific oligonucleotides (Genset Pacific Pty. Ltd), or 0.2 mmol/liter of acidic ribosomal phosphoprotein (36B4), 125 μmol/liter of dNTP in 10× PCR buffer (Geneworks) and water in a total reaction volume of 25 μl. Cycling parameters (30 cycles) were 94°C for 5 min, 94°C for 30 s, and annealing (45 s) of CTR at 62°C, of Cath K at 55°C, of TRAP at 55°C, of Rab3A at 62°C, of Rab3B at 56°C, of Rab3C at 58°C, of Rab3D at 55°C, and of 36B4 at 55°C; 72°C for 40 s; and a final extension step at 72°C for 10 min. Ten microliters of PCR products were separated on a 1.5% agarose gel containing EtBr and photographed.

Protein isolation and immunoblotting. To isolate protein from cultured OCs and RAW 264.7 cells, cells grown as monolayers were washed twice with ice-cold PBS and then lysed in triple lysis buffer containing 50 mM Tris HCl (pH 8), 150 mM NaCl, 0.02% sodium azide, 0.1% SDS, 100 μg/ml phenylmethylsulfonyl fluoride (PMSF), 1 μg/ml aprotinin, 1% Nonidet P40, 0.5% sodium deoxycholate, and a mixture of protease inhibitors (Sigma) at 4°C for 30 min. For total tissue protein extraction, snap-frozen tissues were ground mechanically by mortar and pestle before being lysed for in triple lysis buffer. Both cell and tissue lysates were cleared (12,000 × *g*, 10 min) and resulting postnuclear supernatants (PNS) were resolved by electrophoresis on a SDS–13% polyacrylamide gel and blotted onto a nitrocellulose membrane (Hybond ECL; Amersham Life Science), which was blocked in 5% skim milk in Tris-buffered saline–Tween 20 (TBS-T) for 40 min at room temperature. Enhanced yellow fluorescent protein (EYFP)-tagged proteins were detected using a primary rabbit polyclonal Living Colors A.v. Peptide antibody (anti-EGFP) (1:1,000) dilution (Clontech Laboratories Inc.) or primary rabbit polyclonal Rab3A (K-15) (1:300), Rab3D (1:5,000) or Rab3 (Cl42.1) (1:10,000) antibodies by incubation for 2 h at room temperature. Membranes were washed and incubated with a secondary HRP-conjugated anti-rabbit antibody (Sigma) at a 1:5,000 dilution for 1 h at room temperature. Development was performed using an enhanced chemiluminescent detection kit.

Triton X-114 phase extraction. Triton X-114 extraction of PNS was carried out as described by Bordier (1981) (7). Briefly, RAW 264.7 cell, OC and tissue PNS were adjusted to 1% Triton X-114 and incubated at 4°C for 30 min, layered over a sucrose cushion containing 6% sucrose, 10 mM Tris-HCl (pH 7.4), 150 mM NaCl, and 0.06% Triton X-114, and incubated at 30°C for 5 min. Following centrifugation (300 × *g* for 3 min), the aqueous and detergent phases were collected and adjusted to equal volumes. The detergent phases were subjected to SDS-PAGE and immunoblotted for either EYFP or Rab3 isoforms as described above. Protein concentration was estimated by Bradford assay (Bio-Rad; Hercules, CA).

FISH. For in situ hybridization, PCR was used to generate a cDNA product that encoded the entire open reading frame of murine Rab3D. Amplimers were gel purified and cloned into the pCR2.1 vector using the Original TA Cloning Kit (Invitrogen). All clones were sequenced for the confirmation of gene orientation. Recombinant plasmids containing Rab3D inserts were linearized with BamHI and transcribed into digoxigenin (DIG)-labeled antisense riboprobes with T7 RNA polymerase, using a DIG RNA labeling kit (Boehringer Mannheim, Mannheim, Germany). Fluorescence in situ hybridization (FISH) was performed on OCs derived from neonatal mouse bone imprints, fixed with 4% paraformaldehyde in PBS, under high stringency conditions as described previously in detail (29). Detection of hybridization signal was performed using a fluorescent antibody enhancer kit (Boehringer Mannheim). Signals were assessed by confocal microscopy (Bio-Rad 1000; Bio-Rad).

Mice. Rab3D$^{-/-}$ mice were generated as previously described (59). Littermate controls were used for all experiments. Only female mice were used for quantitative histomorphometric measurements. All animal work was approved by an institutional ethics committee in compliance with the National Health and Medical Research Council (Australia) guidelines.

Bone histology and histomorphometry. Twelve-week-old mice were used for the assessment of bone phenotype. Tibiae and femora were excised, cleared of soft tissue, fixed in 2% paraformaldehyde containing 0.5% glutaraldehyde in 0.1 M phosphate buffer overnight, and decalcified in 8% EDTA for at least 10 days. Consecutive histological sections up to 20 slices per bone were stained with either hematoxylin and eosin (H&E) or tartrate-resistant acid phosphotase histochemistry. Histomorphometric analysis of the secondary spongiosa was performed according to standard methods (54). Statistical differences between groups were assessed by Student's *t* test.

Transmission electron microscopy. Transmission electron microscopy was carried out essentially as described by the methods of McHugh et al. (44) but with minor modifications. Briefly, long bones from 4- to 5-day-old Rab3D$^{-/-}$ and Rab3D$^{+/+}$ littermates were dissected free of soft tissue and fixed with 2.5% glutaraldehyde, 4% paraformaldehyde in 0.01 M cacodylate buffer (pH 7.3) for at least 1 h at room temperature. After removal of the fixation solution, bones were decalcified for 5 days in 14% EDTA (pH 7.4) containing 0.1% glutaraldehyde. Subsequently, bones were washed, postfixed with 1% osmium tetroxide, dehydrated in ethanol, and embedded in Epon 812. Ultrathin sections were counterstained with lead citrate and examined with a Phillips CM 120 Biotwin transmission electron microscope (Phillips Inc, Eindhoven, The Netherlands).

Generation of stable RAW 264.7 cell lines expressing EYFP-Rab3D proteins. An EYFP-Rab3D fusion protein construct was generated by excising a full length Rab3D insert from a pBTM 116 expression vector with EcoRI and SalI and sub-cloning the cDNA into the EcoRI and XhoI sites of the cytomegalovirus (CMV) driven mammalian expression vector pcDNA 3.1 (+) (Invitrogen). An approximately 700 bp region from the pEYFP vector was amplified using primers (+) 5′-ATGATTACGCCAAGCTTG-3′ and (−) 5′-CGGAATTCCTTGTACA GC-3′ to remove the TAA stop codon and insert a downstream EcoRI restriction site. The amplified fragment was subcloned into a pCR2.1 TA cloning vector as outlined in the manufacturer's instructions (Invitrogen). The EYFP-EcoRI insert was ligated into the BamHI and EcoRI sites of the pcDNA 3.1-Rab3D containing expression vector. An EYFP expression vector was subsequently generated by excising the EYFP-EcoRI cDNA insert from the pCR2.1 TA cloning vector with BamHI and EcoRI and subcloning it into the pcDNA 3.1 mammalian expression vector. A myc-tagged mouse Rab3DQ81L vector, kindly provided by Romano Regazzi (30), served as a template for the construction of a Rab3DQ81L active mutant using a forward primer Q81L (5′GGAATTCCG GATGGCATCCGCTAGTGA-3′) in combination with oligonucleotides corresponding to the bovine growth hormone (BGH) polyadenylation sequence present in the vector (5′TAGAAGGCACACTCGAGG3′). A Rab3DN135I mutant was constructed by PCR using primers (GENSET Pacific PTY. Ltd) containing a single nucleotide exchange leading to an amino acid exchange (N135I) of the gene product. Forward primer (5′-ATCCTCGTGGGGATTAAGTGTG ACCTG-3′) and reverse primer (5′CAGGTCACACAC TTAATCCC CACGA GGAT-3′) were used. A Rab3DΔCXC mutant was established by deletion of the last 3 amino acids (CSC) using a reverse primer 5′-GCTCTAGAGCTAGCTG CTCGGCTGTGG-3′ paired with the EYFP forward primer. Wild-type Rab3D fragments were excised from the pcDNA 3.1-EYFP vector and replaced by PCR fragments containing the various mutations. All constructs were sequenced to ensure fidelity of ligation and mutations.

To generate stable cell lines, expressing EYFP-Rab3D wild-type and mutant RAW 264.7 cells were transiently transfected by electroporation essentially as described previously (67) except that 20 μg of plasmid DNA was used for the transfection. After a 24-h recovery period, transfected cells were cultured in selection media containing 500 μg/ml geneticin (G418; Sigma) for 2 weeks. Colonies resistant to the antibiotic were selected, expanded and expression levels monitored using a combination of immunoblotting, FACS analysis, and confocal microscopy. For fluorescence-activated cell sorting (FACS), the cells were washed with PBS, trypsinized, pelleted, and resuspended in complete α-MEM (20% FBS) for sorting by a Facstar Plus cytometer (Becton Dickinson). Cell lines were routinely resorted to maintain the homogeneity of the populations.

GTP-binding assay. Binding of [α-P^{32}]GTP to proteins blotted on nitrocellulose membrane was carried out in accordance to the protocol of Bucci et al. (9). Briefly, whole cell lysates were subject to SDS-PAGE and transferred to nitrocellulose membranes, which were incubated in binding buffer (50 mM sodium phosphate, pH 7.5, 10 μM $MgCl_2$, 2 mM dithiothreitol [DTT], 0.2% Tween 20, 4 μM ATP) for 30 min at room temperature, and then probed with 1 μCi/ml [α-P^{32}]GTP (Amersham Life Sciences) in binding buffer for 2 h. After four 15 min washes with binding buffer, the blot was wrapped wet and exposed to film for 16 h and then subsequently stripped and processed for immunoblotting with rabbit polyclonal anti-Rab3D antibodies.

Fluorescence and time-lapse confocal microscopy. RAW 264.7 cells and OCs grown on glass coverslips were washed twice with PBS and fixed with 4% paraformaldehyde in PBS, pH 7.2, for 15 min. Subsequently, cells were incubated for 5 min in 0.2% Triton X-100 in PBS. Following permeabilization, cells were washed in PBS containing 2% bovine serum albumin (BSA) and labeled with primary antibodies for 45 min at room temperature. After extensive washing with PBS, primary antibodies were detected by goat anti-mouse, goat anti-rabbit, or sheep anti-chicken immunoglobulin G conjugated to either Alexa Fluor 488 or 546 (Molecular Probes Inc.) at a dilution of 1:1,000. After 30 min of incubation, cells were washed in PBS and mounted onto slides in low fade mounting medium (25% glycerol, 15% polyvinyl alcohol in Tris-PO_4, pH 8.5). For the detection of F-actin microfilaments, cells were fixed and permeabilized as described above and incubated with rhodamine-conjugated phalloidin (1:100; Molecular Probes Inc.) for 2 h at room temperature. Cell nuclei were visualized by counterstaining with Hoechst dye (1:10,000; Molecular Probes Inc.). In some experiments, cells

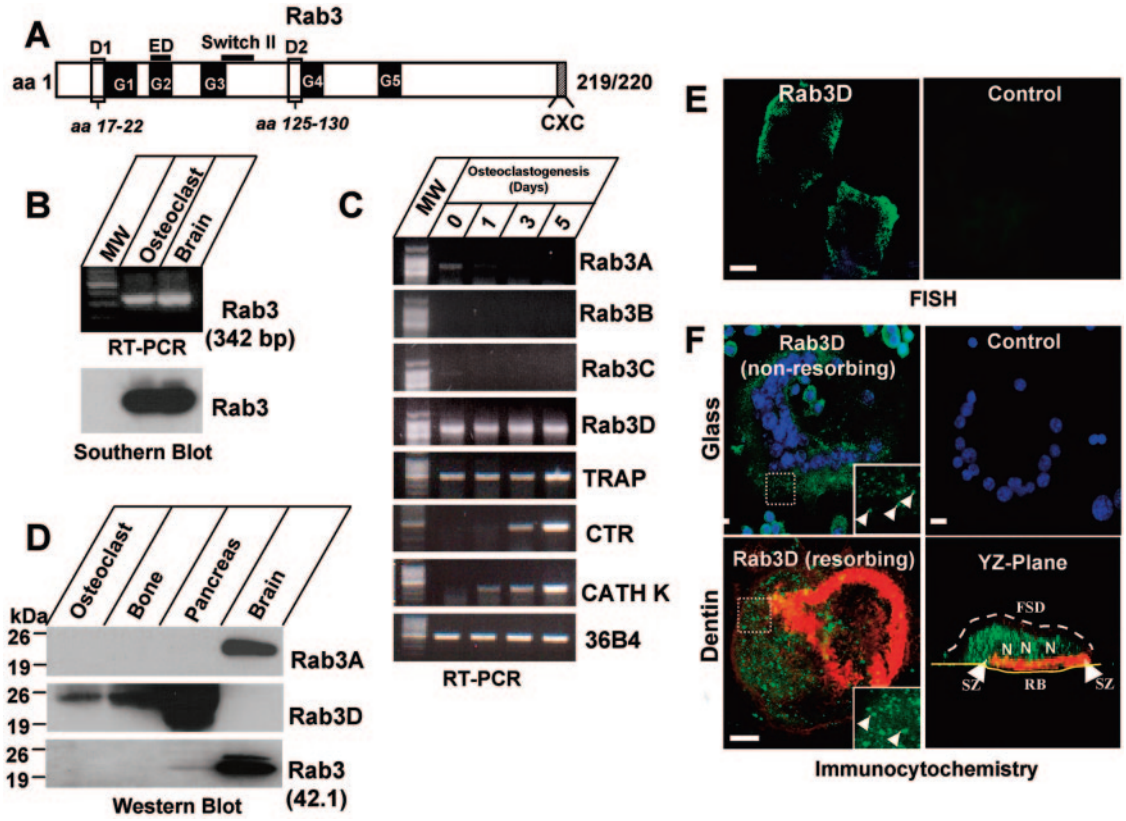

FIG. 1. Expression of Rab3 isoforms in mouse osteoclasts. (A) Schematic representation of the RT-PCR strategy using degenerative Rab3 oligonucleotides coding for regions D1 and D2. Conserved structural domains between Rab and Ras proteins are designated G1-G5. ED denotes effector-binding loop. The hatched region represents the membrane-binding motif (CXC). (B) Detection of Rab3 GTPases in BMM-derived OCs by degenerative RT-PCR and Southern blot analysis. Sizes (in base pairs) were determined using DNA molecular weight (MW) standards. Brain served as a positive control for Rab3 mRNA expression. Southern blotting was perform under high stringency conditions using an α-P^{32}-labeled mouse Rab3 probe as outlined in the Materials and Methods. (C) mRNA expression and regulation of Rab3 isoforms in RANKL-differentiated RAW 264.7 cells. RAW 264.7 cells were cultured in either the presence or absence of RANKL (100 ng/ml) for 0 to 5 days before being harvested for mRNA extraction. cDNA was synthesized using 2 μg of purified mRNA and then subjected to PCR amplification using gene specific primers to mouse Rab3A, Rab3B, Rab3C, Rab3D, TRAP, Cath K, CTR and the internal control 36B4. (D) Immunodetection of Rab3 proteins in OCs and bone. OC and tissue homogenates were extracted with Triton X-114 to enrich for Rab3 proteins that carry C-terminal geranylgeranyl modification. Proteins (OC, 100 μg; bone, 100 μg) were analyzed by SDS-PAGE and immunoblotting with antibodies directed against Rab3A (K-15), Rab3D and Rab3/A/B/C (42.1). Pancreas (50 μg) and brain (10 μg) serve as positive controls. (E) Cellular localization of *Rab3D* gene transcripts in primary mouse OCs by FISH. Rab3D mRNA transcripts are evidenced by the green (FITC) hybridization signal. In situ hybridization following RNase treatment show only background activity and served as a control. (F) Immunolocalization of Rab3D in nonpolarized and highly polarized OCs. Isolated mature OCs were seeded onto either glass or dentin slices and cultured overnight before being fixed and immunostained with primary polyclonal rabbit anti-Rab3D antibodies and secondary anti-rabbit antibody–Alexa 488 nm (green). Nuclei and filamentous actin were visualized with Hoechst staining (blue) and rhodamine-labeled phalloidin (red), respectively. Bar, 10 μm.

were incubated at 37°C with rhodamine-β dextran (10,000 molecular weight; 50 μg/ml) for 4 h, Alexa Fluor 546-transferrin (20 μg/ml) for 30 min, or the fixable acidotropic probe Lysotracker Red DND-99 (100 nM) for 30 min (all from Molecular Probes Inc.) before being fixed and processed for microscopy. Fluorescence-based TRAP staining was performed according to the established methods of Filgueira and outlined in detail in reference 21.

Detection of fluorochromes was carried out by confocal laser scanning microscopy (CLSM) (MRC-1000; Bio-Rad), equipped with a krypton-argon laser or argon ion laser coupled to an epifluorescence Nikon Diaphot 300 inverted microscope. For the detection of immunofluorescent staining and EYFP-signal, both 60× oil immersion objective lens (Nikon; numerical aperture = 1.6) and 40× UV oil immersion objective lens (Nikon; numerical aperture = 1.2) were used. Forty serial optical sections (z = 0.1 μm) were acquired satisfying the Nyquist criteria for sampling. In some cases, individual OCs cultured on bone slices were assessed throughout the entire cell using serial optical sections (1-μm intervals). The serial optical sections (z-series) from each cell were collected for the construction of three-dimensional images.

For time-lapse microscopy, cells were grown on 8-well Coverglass chamber slides (Nalge, Nunc International) in complete medium buffered with HEPES (20 mM, pH 7.5) (Sigma H-3375) and mounted on a heated stage at 37°C. Serial images were taken at 5-s intervals for 10 min, and stacks were played as AVI files. Confocal sequences were collected as Bio-Rad PIC files and were converted to bitmaps for use in either Scion Imaging software (NIH) or Confocal Assistant 4.02. Images were collected with nonsaturating conditions set up by the use of an output look-up table (LUT).

RESULTS

Rab3D is the predominant Rab3 isoform expressed in mouse osteoclasts. Following an earlier report (1) in which only Rab3A and Rab3B/C isoforms were detected in OCs, we employed a combination of complementary molecular, biochemical, and cell biological approaches to examine expression of Rab3 mRNA and protein expression in the same cells and their mononuclear precursors. First, degenerative oligonucleotide primers based on conserved Rab3 family sequences (Fig.

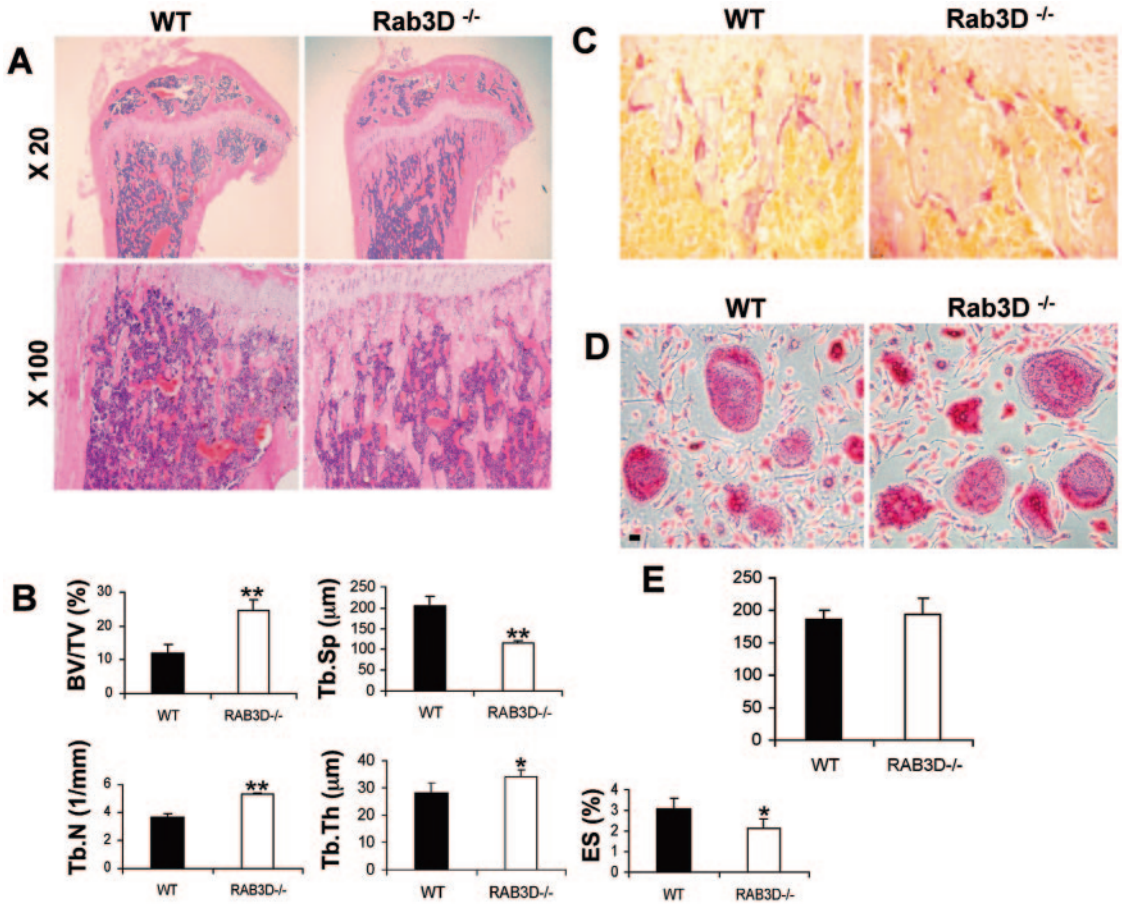

FIG. 2. Osteopetrosis in Rab3D$^{-/-}$ mice (A) Representative longitudinal sections of distal tibae from 12-week-old, sex-matched wild-type (WT) and Rab3D$^{-/-}$ mice stained with hematoxylin and eosin. More dense and irregular shaped trabecular bone was observed in the metaphyseal region of Rab3D$^{-/-}$ mice but not WT controls. (B) Histomorphometric analysis of tibial bone architecture. Trabecular bone volume (BV/TV), trabecular number (Tb.N), trabecular separation (Tb.Sp), trabecular thickness (Tb.Th), and eroded surface (ES). Data are expressed as means ± SEM. (*, $P < 0.025$; **, $P < 0.001$). Results from five mice of each genotype are shown and were measured blindly. (C) Histologic sections of tibial metaphysis of WT and Rab3D$^{-/-}$ littermates stained for TRAP activity (red reaction product) to visualize OCs in vivo (×200). (D) Normal ex vivo OC formation in Rab3D$^{-/-}$ mice. BMMs from either WT or Rab3D$^{-/-}$ 6-week-old female mice were cultured for 7 days in the presence of M-CSF (20 ng/ml) and RANKL (100 ng/ml) before being fixed and stained for TRAP. Note multinucleated cells derived form Rab3D$^{-/-}$ BMMs are indistinguishable from those derived from that of the WT. Bar, 10 μm. (E) Quantitation of TRAP positive multinuclear cells (>3 nuclei) following a 7-day BMM/RANKL/M-CSF culture. Bars represent means ± standard errors of the mean ($n = 6$).

1A; D1:QNFDYM = RabS1; D2:WDNAQV = RabS3) were used to selectively amplify Rab3 cDNAs from bone marrow monocyte-derived OCs. Brain cDNA was added as a positive control because this organ is known to abundantly express Rab3 proteins (24). As shown in Fig. 1B, a 342-bp fragment corresponding to the predicted size for Rab3 GTPases was amplified from both OC and brain cDNA. Southern blot analysis using a α-P^{32}-labeled mouse Rab3 probe confirmed the identity of these products as Rab3 proteins. Cloning and sequence analysis revealed that the majority of clones (80%) encoded mouse Rab3D, as documented by their identity with the published sequence of mouse Rab3D (4). Similar results were obtained using OCs obtained by RANKL-differentiated RAW 264.7 cells. (Fig. 1C). Moreover, Rab3A and Rab3C message is weakly expressed and confined to the early stages of RANKL differentiation, while Rab3D expression is strong and constitutive throughout osteoclastogenesis.

To confirm the PCR data, we next assessed Rab3 protein expression levels in OCs by immunoblotting using a number of well-characterized Rab3 specific antisera. When total protein extracts were tested, we found that the endogenous expression of Rab3 proteins was low and near the detection limit (unpublished data). Geranylgeranylation (prenylation) is a posttranslation lipid modification that is required for the binding of Rab proteins to their target membrane(s) (66), thus rendering Rabs hydrophobic and enabling them to be copurified with membrane proteins by Triton X-114 partition (7, 20, 33). We used these facts to circumvent the difficulty of detecting Rabs in whole cell lysates, by enriching for geranylgeranylated Rab3 proteins with Triton-X-114, which selectively concentrates membrane fractions. Figure 1D shows representative immunoblots of Rab3 proteins performed on Triton X-114 enriched fractions of RAW 264.7 cell-derived OCs, bone, pancreas, and brain. Brain and pancreas served as positive controls, as they exhibit high levels of Rab3A/B/C and Rab3D, respectively (63, 76). In agreement with our PCR analyses and corresponding to the published molecular weight, Rab3D is present in OCs as a 27-kDa peptide that comigrates with the pancreas control. The

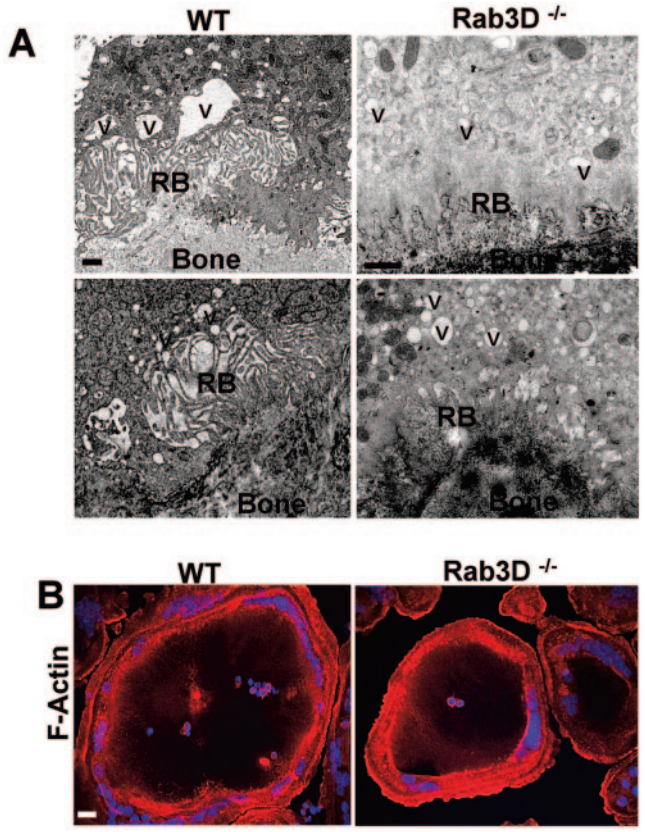

FIG. 3. (A) Disturbed ruffled border formation in OCs of Rab3D$^{-/-}$ mice. Representative electron micrographs of OCs resident in metaphyseal bone of two individual WT and Rab3D$^{-/-}$ mice. Note whereas the ruffled borders of WT OCs exhibit characteristic villus-like projections, those of Rab3D$^{-/-}$ are irregular and blunted. Bar, 1 μm. (B) Normal actin organization in Rab3D$^{-/-}$ OCs. BMMs from WT and Rab3D$^{-/-}$ mice were cultured on glass coverslips for 7 days in the presence of M-CSF (20 ng/ml) and RANKL (100 ng/ml). Multinucleated cells were then fixed, permeablized, and stained with rhodamine-phalloidin (red) to visual F-actin (red) and Hoechst to identify nuclei (blue). Bar, 10 μm.

same band is also evident in total bone extracts. In comparison, immunoblotting using the polyclonal Rab3A antiserum failed to detect significant levels of Rab3A expression in either OCs or bone using equivalent amounts of protein, although it is abundant in brain. While individual detection of Rab3B and Rab3C isoforms is precluded due to the lack of appropriate reagents, the monoclonal 42.1 Rab3 antibody, which recognizes Rab3A/B/C, fails to detect significant levels of these Rab3 proteins in OCs and bone but visualizes strong levels in control brain lysates. We also find that the 42.1 antibody reacts with Rab3D, albeit weakly, in highly expressing pancreatic tissue (Fig. 1D). Interestingly, minimal Rab3 signal is detectable in aqueous/cytosolic fractions of OC protein extracts (unpublished data) indicating that endogenous Rab3 proteins are membrane-affiliated in these cells.

Having established that Rab3D is the predominant Rab3 isoform expressed in OCs, we next confirmed its existence in authentic mouse OCs. To this end, primary OCs were isolated from the long bones of neonatal mice and probed for Rab3D using fluorescence in situ hybridization (FISH) and immunocytochemical methods. As shown in Fig. 1E, Rab3D mRNA is present throughout the cytoplasm of mature OCs, which also are positive for TRAP following double staining (unpublished data). RNase treatment prior to hybridization resulted in loss of signals in all cells, indicating the specificity of the probe for its target mRNA sequence. Rab3D protein is also detected throughout the cytosol in OCs when stained with Rab3D-specific antisera in both nonresorbing and highly resorbing OCs (Fig. 1F). Consistent with its membrane association, Rab3D (green) is localized to small punctate structures ranging in size from approximately 100 to 500 nm. These compartments are randomly distributed throughout the cytosolic compartment but appear concentrated within the juxtanuclear/Golgi region (nuclei in blue). Low levels of diffuse immunofluorescence are also detected in the cytosol, probably reflecting the unprenylated pool of Rab3D. Importantly, no appreciable staining is observed in the absence of Rab3D antisera or when OCs were treated with preimmune serum at equivalent dilution. In actively resorbing cells, identified by characteristic sealing zone formations (red), Rab3D-bearing vesicles show no obvious sign of polarized targeting to either the ruffled border or basolateral membrane domains. Thus, based on these data, we conclude that Rab3D, rather than Rab3A/B/C, is major Rab3 species expressed in mouse OCs.

Mice lacking Rab3D manifest a phenotype of osteopetrosis. The abundance of Rab3D in OCs suggests that this GTPase may play an important role in the physiology of these bone-resorbing polykaryons. To test this hypothesis, we examined the skeletal architecture of Rab3D-deficient mice. The animals are viable and fertile and do not display any overt phenotypic abnormalities (59). Histological examination of longitudinal sections of the distal metaphyseal regions of tibias reveals a higher trabecular bone volume in Rab3D$^{-/-}$ mice compared to wild-type (WT) littermates (Fig. 2A). In particular, the spatial organization of the trabecular bone network is dense and irregular within the metaphysis of Rab3D$^{-/-}$ animals as compared to their WT counterparts. Reflecting these morphological aberrations, histomorphometric parameters of decalcified tibial sections reveal that the volume of the trabecular bone (BV/TV) in the Rab3D knockout (KO) mice is increased more than two fold compared to WT mice (Fig. 2B). Consistent with this finding, both trabecular number (Tb.N) and thickness (Tb.Th) are increased by more than two-thirds in mice lacking Rab3D. In addition, trabecular separation (Tb.Sp) and total eroded surface (ES) are markedly lower in the bones of Rab3D$^{-/-}$ animals. In contrast, there is little detectable difference in cortical bone thickness and epiphyseal architecture (unpublished data), suggesting no obvious effect of Rab3D on bone formation by osteoblasts in vivo. Together these histomorphometric results indicate that mice lacking Rab3D are osteosclerotic.

The decreased total eroded surface suggested that the bone defect may reflect a deficiency in OC formation and/or activity. To distinguish between these possibilities we stained bone sections for TRAP activity, an index of OC number in vivo. Visual inspection reveals no obvious differences in OCs residing in the bone metaphysis (Fig. 2C). To gain a more accurate assessment of osteoclastogenesis, OC precursors, in the form of BMMs, were cultured ex vivo for 7 days in the presence of optimal concentrations of RANKL and M-CSF. As shown in

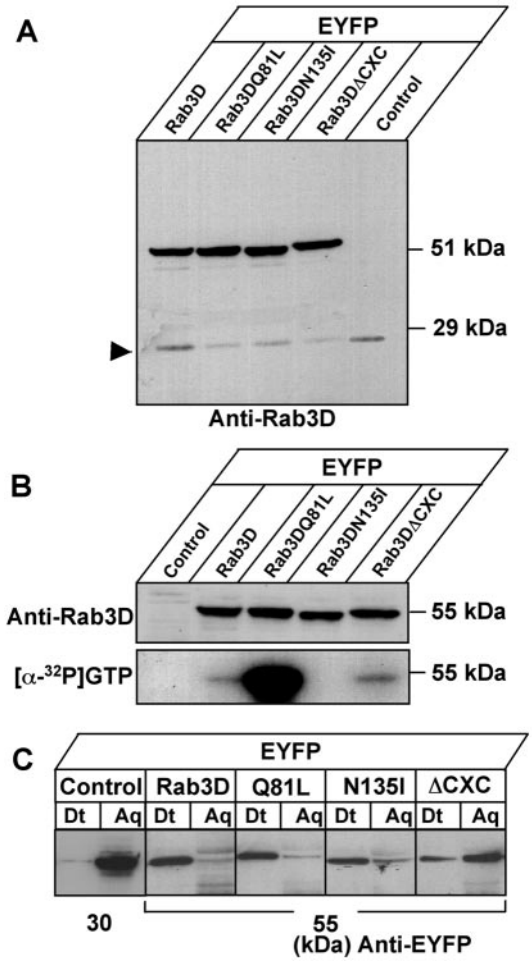

FIG. 4. Expression and biochemical characterization of stably expressed EYFP-Rab3D fusion chimeras in RAW 264.7 cells. (A) Western blot analysis of lysates of RAW 264.7 cells transfected with pEYFP and pEYFP-Rab3D, -Rab3DQ81L, -Rab3DN135I and -Rab3DΔCXC. Stably transfected RAW 264.7 cells were lysed in standard sample buffer, and 50 μg of total cell lysate was loaded for SDS-PAGE and subsequently transferred onto a nitrocellulose membrane. Incubation was performed using a polyclonal anti-Rab3D antibody, and bands were visualized by the ECL detection system. The arrowhead denotes endogenous Rab3D protein. (B) GTP-binding blot of Rab3D WT and mutant proteins. Nitrocellulose membranes were probed with either radiolabeled [α-^{32}P]GTP for 1 h or a polyclonal anti-Rab3D antibody and subjected to autoradiography and chemiluminescent development. (C) Geranylgeranylation of EYFP-tagged Rab3D fusions. RAW 264.7 cells expressing EYFP, EYFP-Rab3D, or EYFP-Rab3D mutants were lysed in Triton X-114 to examine post-translational processing. The lysates, normalized for protein content, were warmed to 33°C, and the detergent (Dt) and aqueous (Aq) phases were separated by centrifugation as described in Materials and Methods. Equal proportions of each fraction were resolved by SDS-PAGE and immunoblotting using an anti-EGFP (A.v. peptide) serum. EYFP is hydrophilic and partitions almost exclusively into the aqueous phase, whereas geranylgeranylation of the CXC motifs of EYFP-Rab3D, EYFP-Rab3DQ81L, and EYFP-Rab3DN135I imparts sufficient hydrophobicity to partition the proteins into the detergent phase. Truncation of the CXC motif for EYFP-Rab3DΔCXC largely results in partitioning to the aqueous phase. Prenylation is complete, since all of the expressed EYFP-Rab3D and its GTP/GDP-mutants shifted to the detergent phase. All results shown are representative of at least three independent experiments.

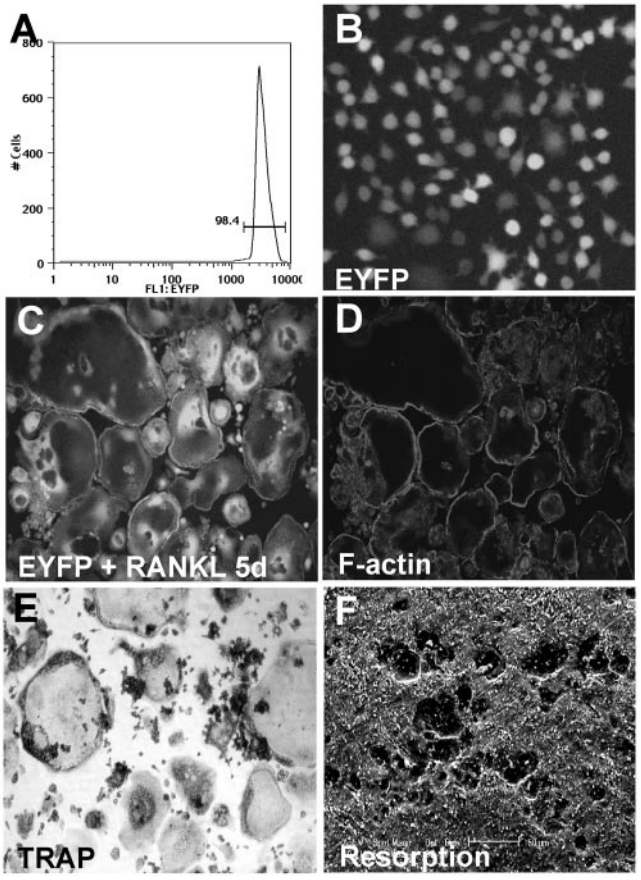

FIG. 5. EYFP-expressing RAW 264.7 cells differentiate into functionally authentic osteoclasts. (A) FACS analysis of postsorted stable expressing EYFP-RAW 264.7 cells. (B through F) EYFP RAW 264.7 cells were stimulated with RANKL to induce differentiation. After 5 days, fully differentiated OCs were either examined by confocal microscopy to compare EYFP expression levels with their mononuclear precursors (B and C) or stained with rhodamine-conjugated phalloidin to visualize F-actin rings (D). (E) TRAP activity of EYFP-expressing OCs. (F) Resorptive pits formed after 9 days of culture on dentin slices.

Fig. 2D, OCs from Rab3D$^{-/-}$ animals form normally. Quantitative analysis reveals no significant difference in OC numbers either in vivo or during in vitro culture between Rab3D KO and WT mice (Fig. 2E). We also failed to detect significant differences in osteoblast bone nodule formation in vitro (unpublished data) which are consistent with the in vivo observations. Taken together, these data indicate that the osteosclerotic phenotype is not related to changes in either OC or osteoblast differentiation.

Since the ability of OCs to resorb bone is directly related to their ability to form and sustain a functional ruffled membrane we next used electron microscopy to examine the morphology of the ruffled border in Rab3D null and WT cells for potential anomalies (Fig. 3A). Strikingly, we find that the ruffled borders of OCs derived from Rab3D mutant mice are structurally abnormal. Whereas the ruffled borders of OCs from WT animals exhibit characteristic thin villous architecture, those in Rab3D$^{-/-}$ OCs consistently comprise thick, blunted projections, not unlike those present in β3 null OCs, which are also dysfunctional (44).

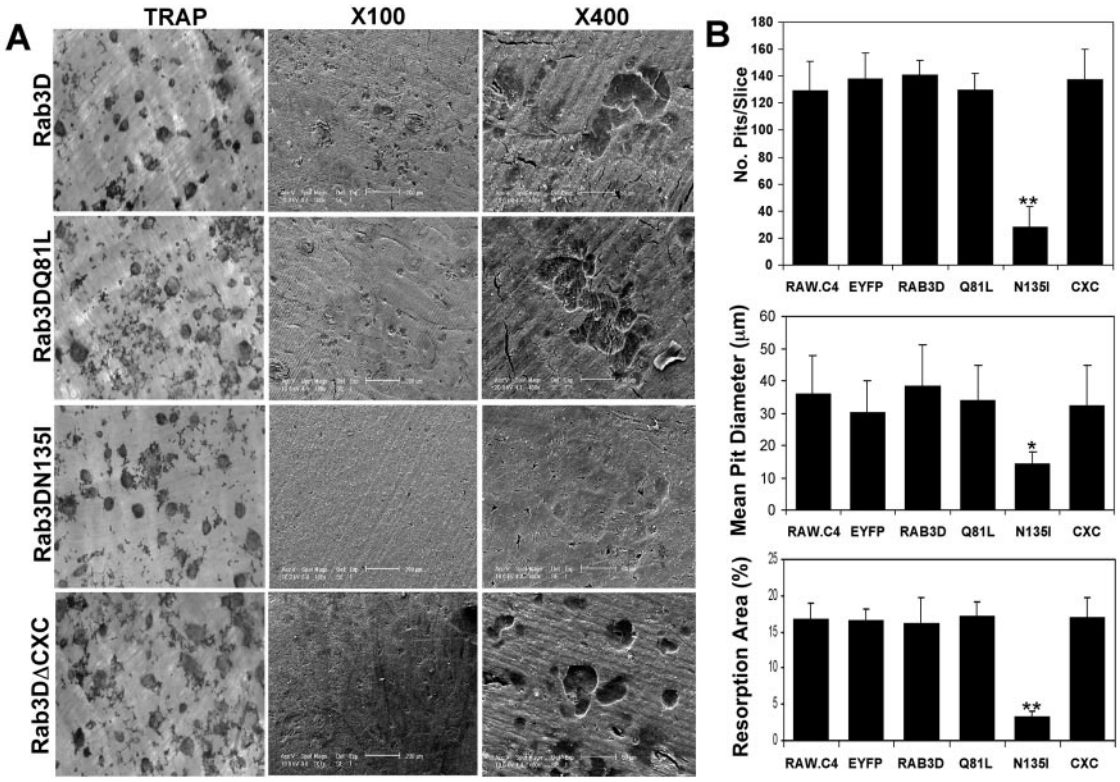

FIG. 6. Overexpression of dominant-negative Rab3DN135I impairs osteoclastic bone resorption in vitro. (A) RAW 264.7 cells stably expressing EYFP-Rab3D and mutant proteins were cultured on dentin slices in the presence of RANKL (100 ng/ml) to analyze resorption activity. After 9 days, TRAP-positive cells were removed and resorptive lacunae were assessed by scanning electron microscopy. Whereas EYFP-Rab3D, constitutively active EYFP-Rab3DQ81L and EYFP-Rab3DΔCXC expressing OCs produce numerous well-defined resorptive lacunae, those formed by EYFP-Rab3DN135I OCs are shallow and poorly demarcated. (B) Resorption parameters of OCs expressing EYFP-Rab3D fusion proteins. Pit number, diameter and percentage resorbed area per dentin slice were examined by scanning electron microscopy. Indices were calculated using image analysis software (NIH). *, $P < 0.05$; **, $P < 0.001$ compared with EYFP in all panels; error bars represent standard deviation of means ($n = 6$).

The formation of the ruffled border coincides with reorganisation of the cytoskeleton. Therefore, we asked if disruption of the ruffled border reflects deficiencies in the OC actin cytoskeleton. To explore this possibility BMMs from wild-type and Rab3D KO mice were cultured in the presence of M-CSF and RANKL. After 7 days, OCs were fixed, permeabilized and stained with rhodamine-phalloidin to visual filamentous actin. As shown in Fig. 3B, OCs from Rab3D-deficient mice display well-organized F-actin rings and podosomes that are comparable to the analogous structures in WT cells, indicating that the ruffled border deficiency is independent of actin cytoskeletal disturbances.

Disruption of osteoclastic bone resorption is dependent on the guanine nucleotide binding, but not prenylation, status of Rab3D. To gain further insight into the mechanisms by which Rab3D regulates osteoclastic bone resorption, we used a mutagenic approach to interfere with GDP/GTP cycling and membrane targeting of Rab3D. Previous studies have shown that substitution of glutamine (Q) at position 81 with leucine (L) within the switch II GTP-binding domain of Rab3D results in a protein that is deficient in GTP hydrolysis and persists in the constitutively active GTP-bound conformation (15, 49, 63). One the other hand, substitution of asparagine (N) at position 135 for an isoleucine (I) in the G4 motif leads to a constitutively inactive protein that has reduced affinity for guanine nucleotides and serves as a dominant-inhibitory mutant (5, 15, 41). Therefore, we constructed constitutively active and inactive Rab3D mutants by site-directed PCR and stably expressed them as enhanced yellow fluorescent protein (EYFP) fusions in RAW 264.7 cells. In addition, we generated a geranylgeranylation mutant (EYFP-Rab3DΔCXC) by truncation of the last three amino acids (CSC) of carboxyl terminal motif that is required for membrane attachment and targeting (14). As a control, a plasmid encoding EYFP alone was also expressed in parallel.

Clones resistant to antibiotic selection were isolated and expanded, and expression levels and transfection efficiencies were assessed by immunoblotting and flow cytometry (Fig. 4 and unpublished data). As shown in Fig. 4A EYFP-fusion chimeras were expressed at equivalent levels and moderately overexpressed compared to the endogenous Rab3D protein. To verify the biochemical characteristics of the fusion chimeras, we next evaluated their GTP-binding properties and geranylgeranylation status. As expected, WT, constitutively active and geranylgeranylation-deficient Rab3D fusion proteins efficiently recruit GTP. On the other hand, GTP-binding affinity is markedly enhanced in cells expressing constitutively active EYFP-Rab3DQ81L, a result that confirms its reduced GTPase activity (Fig. 4B). In comparison, no GTP-binding is detectable for the guanine-nucleotide binding-deficient mutant

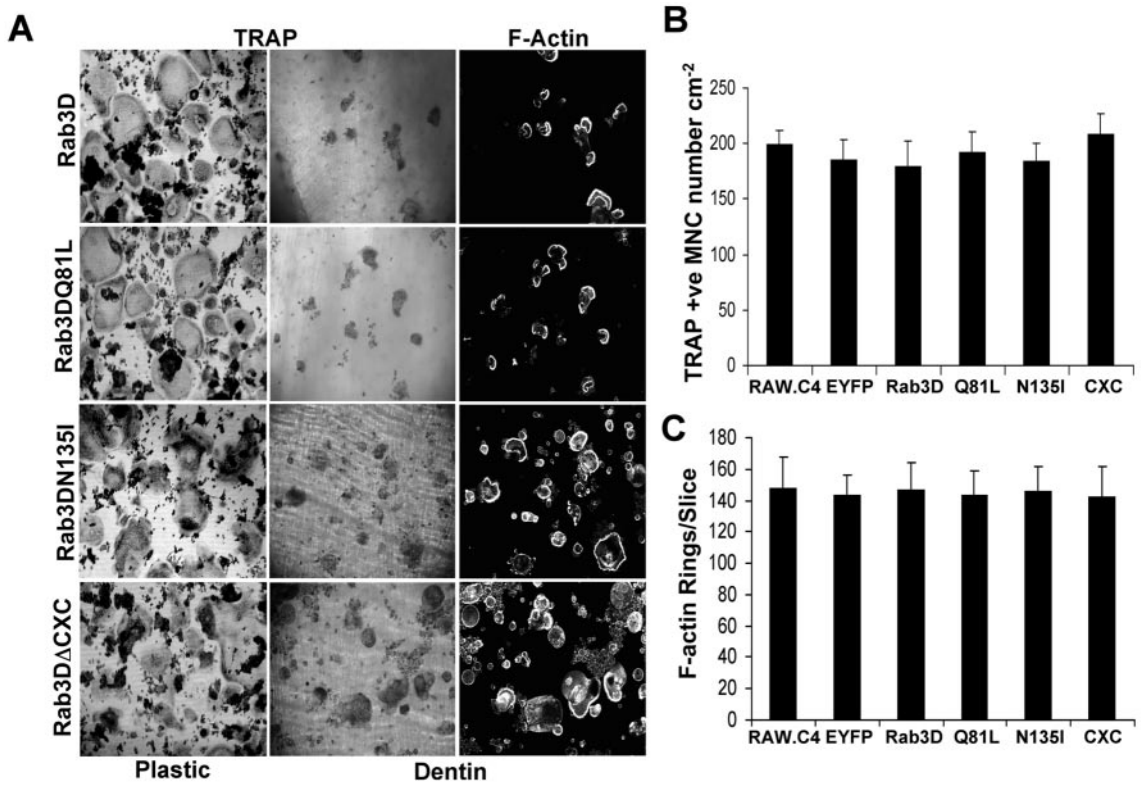

FIG. 7. Overexpression of EYFP-Rab3D and its mutants does not affect osteoclast formation or F-actin organization. (A) Stably transfected RAW 264.7 cells were cultured on plastic or dentin surfaces in the presence of 100 ng/ml RANKL for 5 and 9 days, respectively. OC-like cells were fixed and then stained for either TRAP alone (left panels) or double stained for TRAP and rhodamine-phalloidin (F-actin; middle and right panels) and visualized by bright field and confocal microscopy. Quantitation of the number of TRAP-positive multinucleate cells (>3 nuclei) per cm^2 (B) and number of F-actin rings per dentin slice (C). Error bars represent standard errors of the mean ($n = 6$).

EYFP-Rab3N135I. Likewise, assessment of geranylgeranylation capacity by Triton X-114 phase partitioning revealed that all EYFP-tagged Rab3D fusion proteins, with the predicted exception of EYFP-Rab3DΔCXC, partitioned almost exclusively into the detergent phase (Fig. 4C), indicating that they are efficiently geranylgeranylated when expressed in RAW 264.7 cells.

We also determined whether expression of the EYFP-fusion proteins is sustained during RANKL-induced OC differentiation. As shown in Fig. 5, EYFP expression in RANKL-differentiated OC-like cells is similar to that in its mononuclear progenitors when compared at the same confocal laser settings. Moreover, EYFP-expressing OCs are TRAP positive, form characteristic F-actin rings, and are capable of resorbing bone. Thus, based on these data, we conclude that stable expression of EYFP does not affect OC differentiation and function in vitro.

Having validated the use of EYFP-RAW 264.7 cell system, we next examined the effects of the EYFP-Rab3D fusion chimeras on osteoclastic bone resorption. To this end, WT and mutant EYFP-Rab3D stable RAW 264.7 cell lines were cultured on dentin slices in the presence of RANKL. After 9 days OCs were stained with TRAP and then removed to visualize underlying resorption lacunae by SEM. As shown in Fig. 6A, OCs overexpressing WT EYFP-Rab3D and constitutively active EYFP-Rab3DQ81L resorbed bone with equal efficacy. Expression of the prenylation-deficient mutant, EYFP-Rab3DΔCXC, displayed similar resorptive ability and thus apparently does not interfere with endogenous Rab3D activity. These resorptive phenotypes are comparable to those of the EYFP alone (Fig. 5) and untransfected OC controls (unpublished data). In contrast, overexpression of dominant-negative EYFP-Rab3DN135I impaired osteoclastic bone resorption. Resorption pits of the N135I mutant are typically shallow with poorly demarcated borders. Reflecting these resorptive deficiencies, quantitative analysis reveals that both the number and size of resorptive lacunae is markedly diminished in OCs expressing dominant-negative EYFP-Rab3DN135I compared to all other transfected OCs (Fig. 6B). Furthermore, the percentage of total dentin surface resorbed is significantly lower in OCs transfected with EYFP-Rab3DN135I as compared to control cells. These differing resorptive capacities do not reflect differences in osteoclastogenic abilities of individual RAW 264.7 cell lines, because all stable EYFP-expressing clones were derived from the same parental RAW 264.7 (C4) sub-clone and subjected to equal rounds of passaging. Furthermore, we do not detect any significant differences in osteoclastogenic potential between the stable EYFP-expressing cell lines (Fig. 7A and B), nor do we observe any differences in their ability to activate osteoclastogenic signaling pathways such as RANKL-induced ERK activation (unpublished data). Consistent with our ex vivo observations, we also fail to observe any quantitative morphology differences in the ability to form F-actin rings, with more than 80% of all cells examined pos-

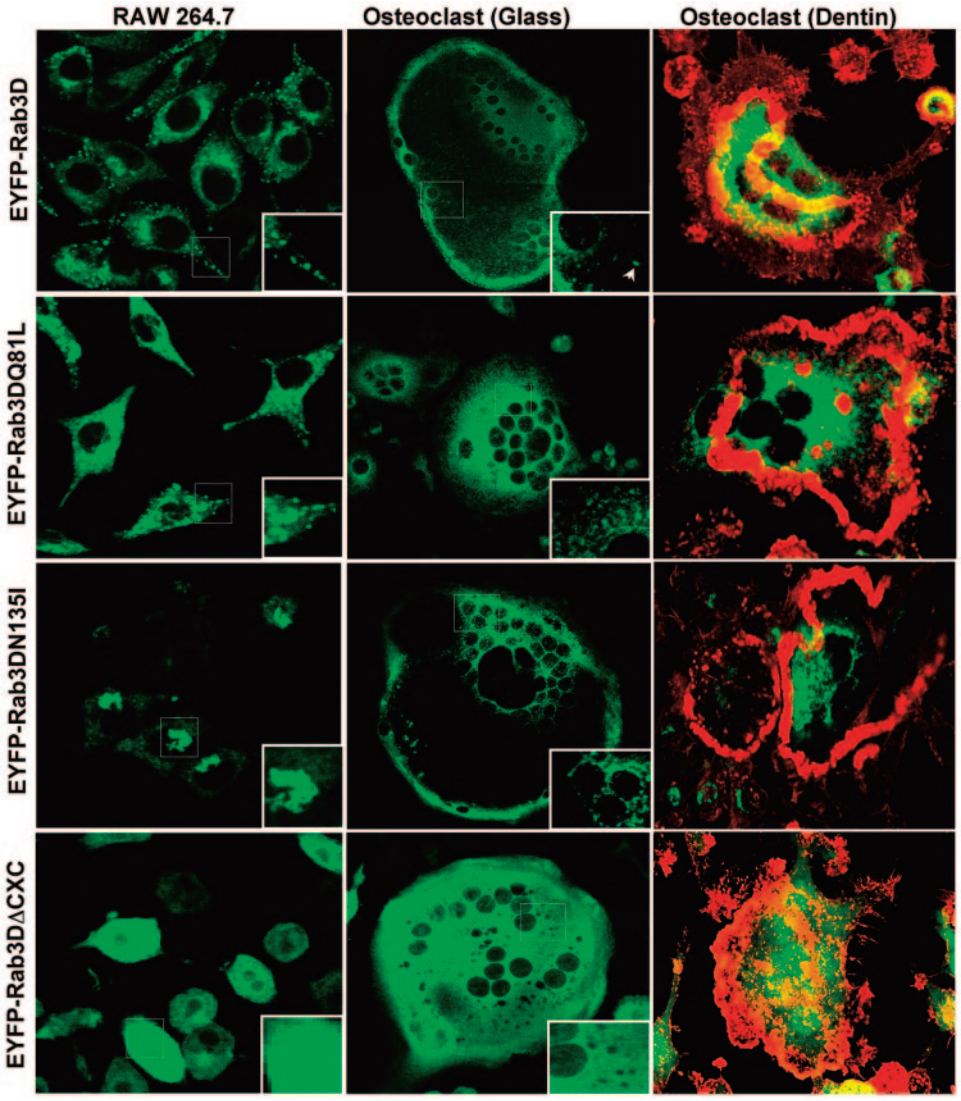

FIG. 8. Subcellular distribution of EYFP-Rab3D fusion proteins in RAW 264.7 cells and osteoclast-like cells. RAW 264.7 cells stably expressing EYFP-Rab3D, EYFP-Rab3DQ81L, EYFP-Rab3DN135I and EYFP-Rab3DΔCXC were grown on either glass coverslips or dentin slices in either the absence or the presence of RANKL (100 ng/ml) for 5 to 9 days. Cells were then fixed with 4% paraformaldehyde and processed for confocal microscopy. Actively resorbing OCs were visualized by the presence of F-actin rings using rhodamine-conjugated phalloidin. Insets represent magnifications of hatched regions. Each image is representative of a 0.4-μm section.

sessing well-defined sealing zones (Fig. 7A and C). Together, our findings indicate that formation of GTP-bound Rab3D, rather than GTP hydrolysis or geranylgeranylation, is the rate-limiting step regulating Rab3D function during osteoclastic bone resorption.

GTP-Rab3D regulates the trafficking and biogenesis of a subset of post-TGN vesicles. To further our analysis of the intracellular events by which Rab3D regulates during bone resorption, we next compared the subcellular distributions of EYFP-tagged Rab3D WT and mutant proteins when expressed at equivalent levels in RAW 264.7 cells and OCs derived therefrom (Fig. 8). In cells expressing WT EYFP-Rab3D protein, the EYFP signal is enriched on small punctata that resemble vesicles or granules, localizing in the immediate perinuclear region and often residing close to the plasma membrane. In mononuclear RAW 264.7 precursors, these punctate domains are particularly prominent at the cellular periphery and within tips of processes that emanate from these cells. A similar pattern of fluorescence is detected in cells expressing constitutively active EYFP-Rab3DQ81L. However, this subcellular localisation varies with the level of EYFP-Rab3DQ81L overexpression. In weakly expressing cells, EYFP-Rab3DQ81L localizes mainly in the perinuclear/Golgi region and on scattered vesicles throughout the cytoplasm, whereas in cells exhibiting strong expression levels of the active mutant, EYFP signal is localized to large vesicular clusters/aggregates (some >1 μm) in the cell periphery, but more concentrated in the perinuclear region. In contrast, dominant negative EYFP-Rab3DN135I associates with a juxta-nuclear Golgi-like structure(s) with lesser fluorescence diffusely detected throughout the cytosol. Predictably, the EYFP-Rab3DΔCXC prenylation-deficient mutant displays diffuse cytosolic fluorescence distri-

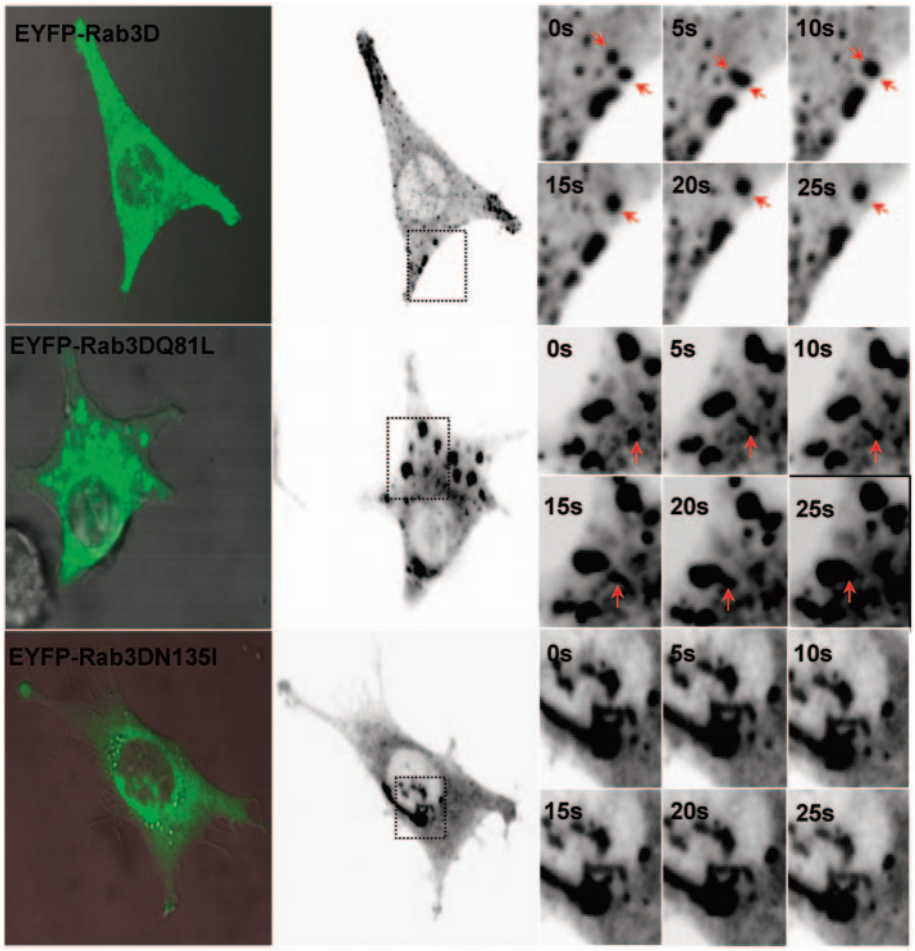

FIG. 9. Rab3D modulates the homotypic fusion of granules in living cells. RAW 264.7 cells expressing either EYFP-Rab3D WT or mutant fusion proteins were cultured on Coverglass chamber slides for 24 h before being analyzed by time-lapse confocal microscopy on a heated stage (37°C). Images were recorded at 5 s intervals for 10 min periods. Left panel illustrates merged phase contrast and EYFP images for each cell. Insets represent enlarged selected images from a time-lapse series. Arrows denote EYFP-Rab3D-bearing vesicles/granules undergoing fusion events. Note little dynamics is observed in EYFP-Rab3DN135I expressing cells (see videos S1 through S3 in the supplemental material).

bution that is comparable to that of EYFP alone. Similar distribution is also observed in transfected COS-1 and PC12 cells (unpublished data), although the size of the Rab3D-postive vesicles varied slightly between the cell types.

While the above data provide information regarding localization of Rab3D in fixed cells, they yield no insight into the dynamic changes of Rab3 proteins. To address this issue we performed time-lapse imaging of live cells. RAW 264.7 cells stably expressing EYFP-Rab3D fusions were cultured on glass chamber slides overnight before being transferred to a temperature controlled stage (37°C) for confocal analysis. Standard imaging conditions used confocal microscopy to collect single confocal slices every 5 s for periods up to 10 min. In this circumstance, Rab3D-bearing vesicles shuttle in a randomized fashion, displaying bidirectional short-range movements within a limited area (less than 3 μm in diameter in 10-min periods). Occasionally we observe homotypic budding and fusion, indicating that these are highly dynamic events (Fig. 9; see also video S1 in the supplemental material). These results did not arise because trafficking structures had moved out of the plane of focus, i.e., "blink-out," because individual homotypic fusions can be continuously tracked for several minutes after vesicle apposition has occurred. Similarly, numerous homotypic fusion events between pleomorphic tubular-vesicular structures and multivesicular aggregates are observed in RAW 264.7 cells expressing the active EYFP-Rab3DQ81L mutant (see video S2 in the supplemental material). In most instances, larger aggregates or clusters displayed limited directional motion and tended to oscillate in live cells. By comparison, little vesicular trafficking is observed in cells expressing EYFP-Rab3DN135I; rather, EYFP signal appeared to be stably retained in the paranuclear (Golgi) region (see video S3 in the supplemental material).

To further dissect the nature of this Rab3D trafficking pathway we performed immunostaining using a panel of well-characterized Golgi, endosomal, and lysosomal compartment markers. RAW 264.7 cells were used for the initial assessment because of their well-characterized subcellular organization. As shown in Fig. 10, WT and active Rab3D partially colocalized with TGN38, a marker of the TGN. This colocalization is accentuated in cells expressing the Golgi-restricted EYFP-Rab3DN135I mutant. In contrast, little to no overlap is ob-

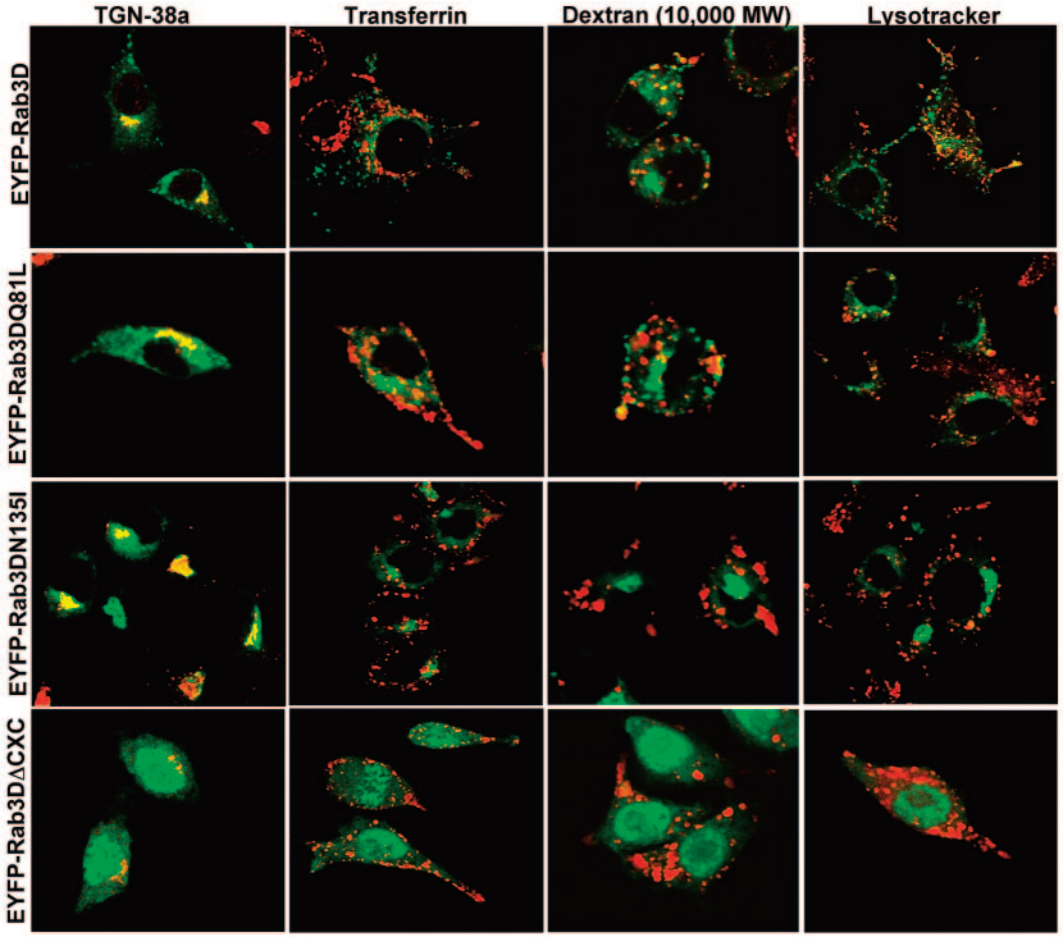

FIG. 10. Rab3D is associated with a nonendosomal/lysosomal post-TGN vesicular compartment. Stably transfected RAW 264.7 cells expressing EYFP-Rab3D fusions were labeled with organelle-specific markers. To visualize the TGN, cells were incubated with anti-TGN38 and Alexa Fluor 546–goat anti-rabbit secondary antibodies. For early and recycling endosomes, cells were loaded with either Alexa Fluor 546-transferrin (30 min) or the fluid phase marker β-rhodamine-dextran (10,000 molecular weight) (4 h) prior to fixation. Acidic compartments were identified with LysoTracker Red. Whereas EYFP-Rab3D partially colabeled with the TGN (yellow), very little overlap can be observed with other endocytic compartment markers.

served with the early/recycling endosome marker transferrin (Alexa fluor 546-tf, 30-min uptake), the fluid phase endosomal marker dextran (Rh-dextran, 10,000 molecular weight, 4-h uptake), and the lysosome-specific vital dye LysoTracker, indicating that Rab3D is not associated with late endosomal and/or lysosomal compartments. Similar localization patterns are observed in RAW 264.7 cell-derived OCs (Fig. 11 and unpublished data).

Finally, to investigate whether Rab3D-bearing vesicles are associated with other established osteoclast-specific markers, we examined the intracellular localization Rab3D in relation to TRAP, a known secreted enzyme which has been shown to localize to transcytotic vesicles (26, 75). As shown in Fig. 12, little to no overlap is observed between large TRAP-positive vesicles and Rab3D, suggesting that Rab3D regulates a vesicle transport pathway that is morphologically and functionally divergent from the intracellular trafficking of TRAP.

DISCUSSION

In the past few years, several lines of evidence hint that Rab GTPases play crucial roles in regulating OC function. Disruption of Rab geranylgeranylation by NE10790 (a bisphosphonate analogue specific to Rab geranylgeranyl transferase) directly inhibits osteoclastic bone resorption, an outcome that correlates with morphological disturbances in vesicle trafficking (17). Antisense oligonucleotide depletion of Rab7, an endosomal/lysosomal related GTPase, impairs osteoclastic polarisation and bone resorption in vitro (81). While it has also been suggested that the Rab3 subfamily plays a role in ruffled border plasmalemma expansion (1), this hypothesis has not been directly tested. In the present study, we document for the first time the existence of a Rab3D-mediated vesicle transport pathway that is required for bone resorption. Attesting to the importance of this trafficking step, disruption of Rab3D activity by either targeted inactivation or expression of dominant-neg-

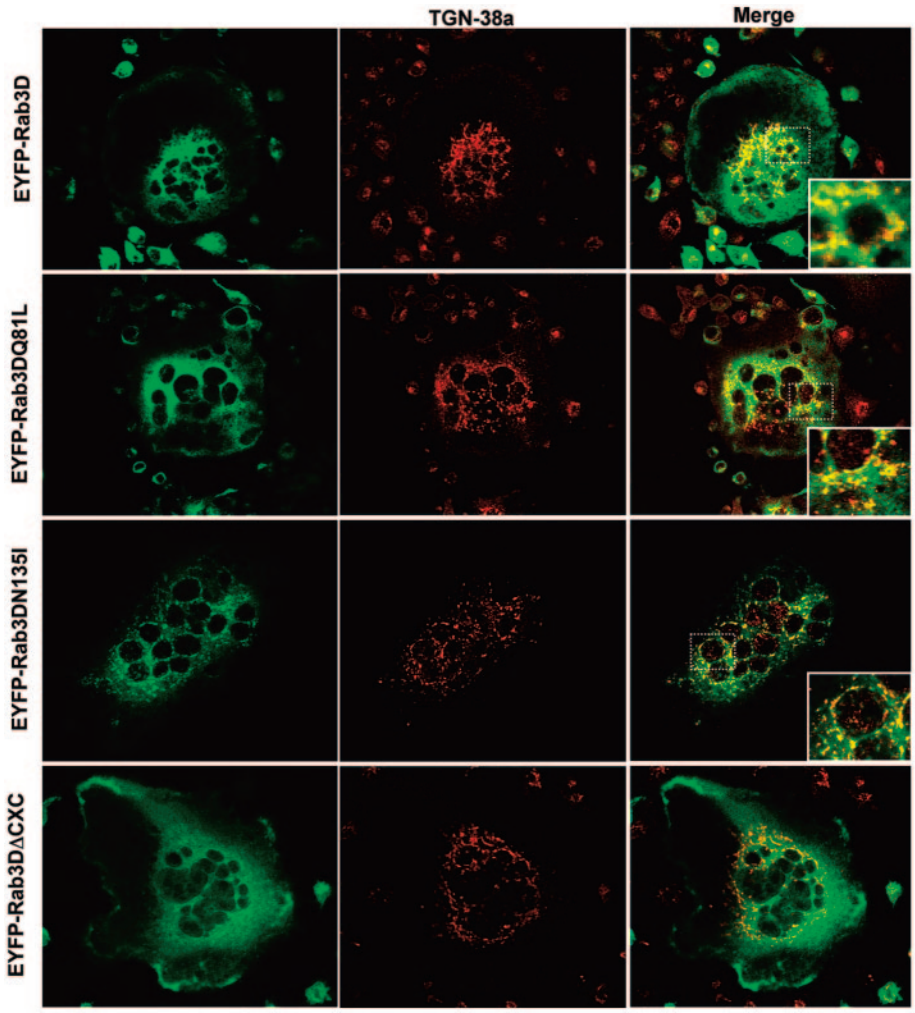

FIG. 11. Colocalization of Rab3D with the TGN in osteoclasts. Stably transfected RAW.264.7 cells overexpressing either EYFP-Rab3D or its mutants were cultured on glass coverslips in the presence of RANKL (100 ng/ml). After 5 days, cells were fixed with 4% paraformaldehyde, permeabilized, and labeled with a rabbit polyclonal rat anti-TGN38 (primary) antibody and Alexa Fluor 546-congated goat anti-rabbit (secondary) antibodies as described in Materials and Methods. Cells were then mounted in low fade mounting medium and analyzed by confocal microscopy. Colocalization depicted by yellow color in merged images. Insets represent magnification of hatched regions.

ative Rab3DN135I leads to significant impairments in osteoclastic bone resorption in vitro and in vivo. Moreover, OCs lacking Rab3D manifest abnormal ruffled borders. Finally, our studies reveal that in OCs, Rab3D associates with and regulate the biogenesis of a subset of post-TGN vesicles that are reminiscent of secretory granules. Together, our data add Rab3D to the list of small GTPases known to regulates OC activity (18) and suggest that this molecule modulates a previously uncharacterized post-TGN trafficking step that contributes to the maintenance of the ruffled border membrane.

Previous studies employing immunoblotting have reported the existence of at least two Rab3 isoforms (Rab3A, Rab3B/C) in murine osteoclastic cells (1). In the present study, using an equivalent culture system, we identified all four Rab3 GTPases by degenerative RT-PCR. Moreover, using a combination of molecular, biochemical, and cell biological methods, we demonstrate that Rab3D, rather than Rab3A/B/C, is in fact the major Rab3 species expressed in mature OCs. The discrepancy between our data and those of Abu-Amer et al. probably results from differences in both culture systems and methods of detection. Thus, the variations in expression profiles might reflect the presence of contaminating bone cell species such as osteoblasts and chondrocytes which have been recently reported to express Rab3A, -B, and -C (6, 55). Furthermore, the 42.1 antibody used in studies of Abu-Amer et al. lacks the specificity to discriminate between Rab3A/B/C/D isoform. In contrast, we used an antibody that uniquely recognizes Rab3D.

The functions of many Rab proteins have been classically dissected by either genetic inactivation in mice and nematodes or the use of interfering mutants (2, 9, 25, 51, 64). Rab3D$^{-/-}$ mice have been recently shown to have enlarged secretory granules in pancreatic acinar cells (59). Our finding that Rab3D$^{-/-}$ mice exhibit an osteosclerotic phenotype extends the physiological importance of GTPases to bone remodeling. The fact that Rab3D$^{-/-}$ mice undergo normal development and yet have a cumulative resorptive defect in vivo indicates that Rab3D is not important during development, but rather plays a role during adult life. This conclusion mimics the com-

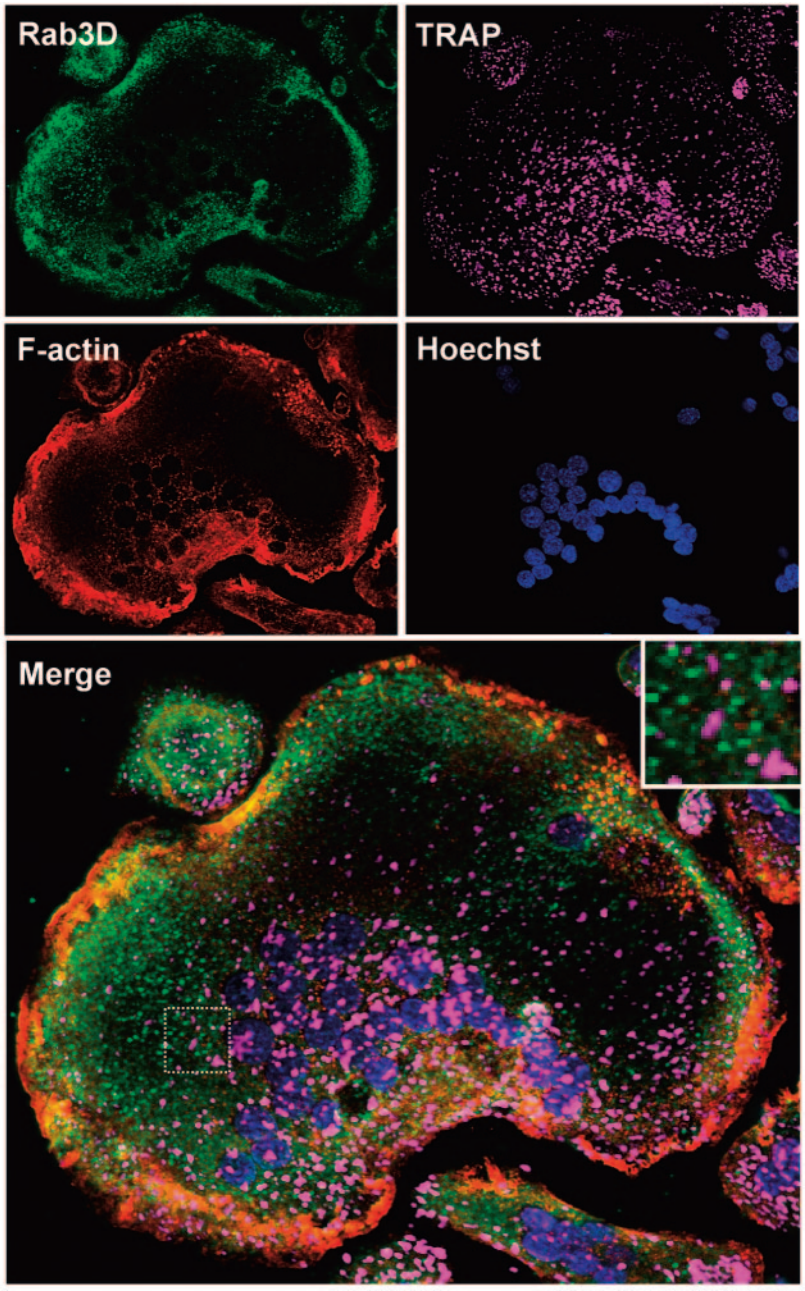

FIG. 12. Intracellular localization of Rab3D and TRAP in osteoclasts. RAW 264.7 cell-derived OCs cultured on glass coverslips were fixed with 4% paraformaldehyde before being stained for TRAP activity (magenta) using a fluorescence-based protocol (see Materials and Methods). OCs were subsequently double immunostained for Rab3D (green), and rhodamine-phalloidin (F-actin, red) before being stained with Hoechst to visualize cell nuclei (blue). Each panel shows a projection image of scanned *x-y* sections through the cell. Merge represents an overlap of all four color channels. Inset represents magnification of hatched region. White color indicates colocalization. Bar, 10 μm.

plex bone phenotypes of mice lacking the β3-integrin, DAP12, Wasp, or NIK, each of which exhibits progressive osteosclerosis (11, 35, 44, 52). In the case of β3, disruptions in OC activity are mirrored by deficiencies in ruffled border formation. Consistent with these earlier observations, ultrastructural analyses in the present study reveals that OCs lacking Rab3D possess similarly disorganized ruffled borders, suggesting that Rab3D may be an important modulator of the ruffled border formation and hence OC function.

Our in vitro mutagenesis studies provide further support for the concept that Rab3D plays a substantial role in bone resorption. Whereas overexpression of WT, constitutively active and prenylation deficient mutants of Rab3D do not exhibit any significant abnormalities, expression of the dominant-negative Rab3DN135I results in a profound impairment of osteoclastic bone resorption. These results are similar to those employing analogous Rab3D mutants in AtT20 cells, mast cells and pancreatic acini (5, 15, 19, 60). It may seem surprising that the

resorptive deficiency in OCs harboring the N135I mutation is greater than to those from Rab3D KO animals. Thus far there has been no simple explanation for this discrepancy; however, it may reflect the differences in the systems employed (loss-of-function mutation verses gene ablation). In the case of Ras, it is now well established that, due to their reduced nucleotide-binding and thus higher tendency to attain a guanosine-nucleotide free state, dominant-inhibitory N-I mutants work by competing with normal endogenous Ras for binding to Ras-activation factors, i.e., Ras GEFs (27, 65, 77). This high affinity results in the formation of "dead-end" complexes, thereby preventing the activation of endogenous Ras by Ras GEF resulting in loss of function. The dominant-negative Rab mutants are thought to function similarly (10, 34, 43). Indeed, recent studies have shown that disruptions in pancreatic secretion are largely attributable to dominant-negative Rab3D mutants' ability to inhibit endogenous Rab3D activation, presumably via sequestering Rab3 GEFs (15, 16). Thus, considering the high homology of Rab3 isoforms, it is likely that sequestering Rab3 GEFs by Rab3DN135I not only disrupts endogenous Rab3D GDP/GTP exchange in OCs but inhibits the activation of other endogenous Rab3 proteins or Rab3-like molecules that may contribute to the resorptive process and thus account for the more pronounced resorptive defect. On the other hand, a single gene deletion in Rab3D-deficent might be compensated, at least partially, by redundancy. This is perhaps best exemplified by the recent phenotypic assessment of Rab3 quadruple KO mice which found that while the absence of all four Rab3 isoforms is lethal at birth, the expression of a single Rab3 allele is sufficient for survival (64).

Another interesting finding is the normal F-actin organization in Rab3D-deficent and mutant OCs, in light of the drastic impairments in ruffled border formation and bone resorption in vitro and in vivo. We interpret this observation to mean that a post-TGN vesicle trafficking step regulated by Rab3D is uncoupled from the cytoskeletal reorganization that accompanies OC attachment and formation of the sealing zone. This hypothesis is supported by two independent studies. First, the recent finding that while GGTOH treatment disrupts Rab activity and inhibits bone resorption in vitro, OCs still maintain their ability to form actin rings, implying that they are not coupled events (17). Second, studies by Saltel et al. (62) reported that OCs retained normal sealing zones following the blockade of Golgi trafficking.

An important step in unravelling the function of a membrane trafficking protein is to define its subcellular localization. Previous localization studies indicate that Rab3D is an established marker of secretory vesicles and granules. For example, Rab3D associates with zymogen granules in the exocrine pancreas (76), dense-core secretory granules in PC12 (41, 42) and AtT-20 cells (5), and β-hexosaminidase-containing granules in mast cells (19, 60, 73). In the present study, we find that Rab3D associates with a unique subpopulation of post-TGN vesicles in OCs and their monocytic precursors. This conclusion is founded on several morphological observations. First, the colocalization between Rab3D and markers of the TGN is consistent with it being a late exocytic carrier vesicle. Second, Rab3D-bearing vesicles, although superficially comparable to endosomes and lysosomes, do not associate with a number of established early or late endocytic/lysosomal markers. Third, Rab3D-bearing vesicles are morphologically distinct from TRAP-containing transcytotic compartments (26, 75). Finally, time-lapse confocal microscopy reveals that Rab3D-bearing vesicles bud dynamically from the TGN and undergo homotypic fusions, an event analogous to immature granule-granule fusions as occur during secretory granule maturation (72). It appears that Rab3D functions as a molecular on/off switch to regulate the biogenesis and/or maturation of these compartments, as such events are blunted by inhibition of Rab3D activity. These findings are consistent with the hypothesis that Rab3D regulates the maintenance and maturation of secretory granules (59). Additional support for this position is provided by recent findings that show expression of dominant-inhibitory mutants of Rab3D impairs the biogenesis of secretory granules in neuroendocrine and endothelial cells (5, 36, 41).

In summary, our results raise the intriguing possibility that Rab3D functions to regulate a previously undocumented, physiologically relevant, rate-limiting post-TGN trafficking step that is required for the maintenance of the ruffled border during osteoclastic bone resorption. Future characterization of the content(s) and nature of these compartments together with the identification of the complement of effector molecules through which Rab3D exerts its regulatory function may uncover potential novel antiresorptive targets for the treatment of OC-mediated bone diseases.

ACKNOWLEDGMENTS

We thank Robert Raffaniello (State University of New York-Health Science Center at Brooklyn, N.Y.) for generously providing Rab3D antibodies and Romano Regazzi (Institut de Biologie Cellulaire et de Morphologie, Lausanne, Switzerland) for the myc-Rab3DQ81L expression vector. All flow cytometry experiments were carried out in the Western Australian Lotteries Commission Flow Cytometry Unit with the assistance of Matthew Wikstrom. Confocal microscopy was carried out at the Western Australian Lotteries Commission Confocal Microscopy Unit at the UWA Department of Pharmacology. Special thanks go to Paul Rigby and Verity Smuts for the assistance with the confocal and scanning electron microscopy and to all members of the Zheng and Jahn laboratories for their insightful discussions.

This research was supported by grants from the National Health and Medical Research Council of Australia and National Institutes of Health awarded to Ming-Hao Zheng (ID9736447), F. Patrick Ross (AR48812 and AR46852), and Steven L. Teitelbaum (AR32788, AR46523, and AR48853).

REFERENCES

1. **Abu-Amer, Y., S. L. Teitelbaum, J. C. Chappel, P. Schlesinger, and F. P. Ross.** 1999. Expression and regulation of RAB3 proteins in osteoclasts and their precursors. J. Bone Miner. Res. **14:**1855–1860.
2. **Alto, N. M., J. Soderling, and J. D. Scott.** 2002. Rab32 is an A-kinase anchoring protein and participates in mitochondrial dynamics. J. Cell Biol. **158:**659–668.
3. **Altschul, S. F., T. L. Madden, A. A. Schaffer, J. Zhang, Z. Zhang, W. Miller, and D. J. Lipman.** 1997. Gapped BLAST and PSI-BLAST: a new generation of protein database search programs. Nucleic Acids Res. **25:**3389–3402.
4. **Baldini, G., T. Hohl, H. Y. Lin, and H. F. Lodish.** 1992. Cloning of a Rab3 isotype predominantly expressed in adipocytes. Proc. Natl. Acad. Sci. USA **89:**5049–5052.
5. **Baldini, G., G. Wang, M. Weber, M. Zweyer, R. Bareggi, J. W. Witkin, and A. M. Martelli.** 1998. Expression of Rab3D N135I inhibits regulated secretion of ACTH in AtT-20 cells. J. Cell Biol. **140:**305–313.
6. **Bhangu, P. S., P. G. Genever, G. J. Spencer, T. S. Grewal, and T. M. Skerry.** 2001. Evidence for targeted vesicular glutamate exocytosis in osteoblasts. Bone **29:**16–23.
7. **Bordier, C.** 1981. Phase separation of integral membrane proteins in Triton X-114 solution. J. Biol. Chem. **256:**1604–1607.
8. **Boyde, A., N. N. Ali, and S. J. Jones.** 1984. Resorption of dentine by isolated osteoclasts in vitro. Br. Dent. J. **156:**216–220.

9. **Bucci, C., R. G. Parton, I. H. Mather, H. Stunnenberg, K. Simons, B. Hoflack, and M. Zerial.** 1992. The small GTPase rab5 functions as a regulatory factor in the early endocytic pathway. Cell **70:**715–728.
10. **Bucci, C., P. Thomsen, P. Nicoziani, J. McCarthy, and B. van Deurs.** 2000. Rab7: a key to lysosome biogenesis. Mol. Biol. Cell **11:**467–480.
11. **Calle, Y., G. E. Jones, C. Jagger, K. Fuller, M. P. Blundell, J. Chow, T. Chambers, and A. J. Thrasher.** 2004. WASp deficiency in mice results in failure to form osteoclast sealing zones and defects in bone resorption. Blood **103:**3552–3561.
12. **Cassady, A. I., A. Luchin, M. C. Ostrowski, and D. A. Hume.** 2003. Regulation of the murine TRACP gene promoter. J. Bone Miner. Res. **18:**1901–1904.
13. **Chambers, T. J., P. A. Revell, K. Fuller, and N. A. Athanasou.** 1984. Resorption of bone by isolated rabbit osteoclasts. J. Cell Sci. **66:**383–399.
14. **Chavrier, P., J. P. Gorvel, E. Stelzer, K. Simons, J. Gruenberg, and M. Zerial.** 1991. Hypervariable C-terminal domain of rab proteins acts as a targeting signal. Nature **353:**769–772.
15. **Chen, X., J. A. Edwards, C. D. Logsdon, S. A. Ernst, and J. A. Williams.** 2002. Dominant negative Rab3D inhibits amylase release from mouse pancreatic acini. J. Biol. Chem. **277:**18002–18009.
16. **Chen, X., S. A. Ernst, and J. A. Williams.** 2003. Dominant negative Rab3D mutants reduce GTP-bound endogenous Rab3D in pancreatic acini. J. Biol. Chem. **278:**50053–50060.
17. **Coxon, F. P., M. H. Helfrich, B. Larijani, M. Muzylak, J. E. Dunford, D. Marshall, A. D. McKinnon, S. A. Nesbitt, M. A. Horton, M. C. Seabra, F. H. Ebetino, and M. J. Rogers.** 2001. Identification of a novel phosphonocarboxylate inhibitor of Rab geranylgeranyl transferase that specifically prevents Rab prenylation in osteoclasts and macrophages. J. Biol. Chem. **276:**48213–48222.
18. **Coxon, F. P., and M. J. Rogers.** 2003. The Role of Prenylated Small GTP-Binding Proteins in the Regulation of Osteoclast Function. Calcif. Tissue Int. **72:**80–84.
19. **Demo, S. D., E. Masuda, A. B. Rossi, B. T. Throndset, A. L. Gerard, E. H. Chan, R. J. Armstrong, B. P. Fox, J. B. Lorens, D. G. Payan, R. H. Scheller, and J. M. Fisher.** 1999. Quantitative measurement of mast cell degranulation using a novel flow cytometric annexin-V binding assay. Cytometry **36:**340–348.
20. **Farnsworth, C. C., M. Kawata, Y. Yoshida, Y. Takai, M. H. Gelb, and J. A. Glomset.** 1991. C terminus of the small GTP-binding protein smg p25A contains two geranylgeranylated cysteine residues and a methyl ester. Proc. Natl. Acad. Sci. USA **88:**6196–6200.
21. **Filgueira, L.** 2004. Fluorescence-based staining for tartrate-resistant acidic phosphatase (TRAP) in osteoclasts combined with other fluorescent dyes and protocols. J. Histochem. Cytochem. **52:**411–414.
22. **Fischer von Mollard, G., G. A. Mignery, M. Baumert, M. S. Perin, T. J. Hanson, P. M. Burger, R. Jahn, and T. C. Sudhof.** 1990. rab3 is a small GTP-binding protein exclusively localized to synaptic vesicles. Proc. Natl. Acad. Sci. USA **87:**1988–1992.
23. **Fischer von Mollard, G., B. Stahl, A. Khokhlatchev, T. C. Sudhof, and R. Jahn.** 1994. Rab3C is a synaptic vesicle protein that dissociates from synaptic vesicles after stimulation of exocytosis. J. Biol. Chem. **269:**10971–10974.
24. **Fischer von Mollard, G., T. C. Sudhof, and R. Jahn.** 1991. A small GTP-binding protein dissociates from synaptic vesicles during exocytosis. Nature **349:**79–81.
25. **Geppert, M., V. Y. Bolshakov, S. A. Siegelbaum, K. Takei, P. De Camilli, R. E. Hammer, and T. C. Sudhof.** 1994. The role of Rab3A in neurotransmitter release. Nature **369:**493–497.
26. **Halleen, J. M., S. Raisanen, J. J. Salo, S. V. Reddy, G. D. Roodman, T. A. Hentunen, P. P. Lehenkari, H. Kaija, P. Vihko, and H. K. Vaananen.** 1999. Intracellular fragmentation of bone resorption products by reactive oxygen species generated by osteoclastic tartrate-resistant acid phosphatase. J. Biol. Chem. **274:**22907–22910.
27. **Hoffenberg, S., L. Nikolova, J. Y. Pan, D. S. Daniel, M. Wessling-Resnick, B. J. Knoll, and B. F. Dickey.** 1995. Functional and structural interactions of the Rab5 D136N mutant with xanthine nucleotides. Biochem. Biophys. Res. Commun. **215:**241–249.
28. **Holz, R. W., W. H. Brondyk, R. A. Senter, L. Kuizon, and I. G. Macara.** 1994. Evidence for the involvement of Rab3A in Ca(2+)-dependent exocytosis from adrenal chromaffin cells. J. Biol. Chem. **269:**10229–10234.
29. **Huang, L., J. Xu, D. J. Wood, and M. H. Zheng.** 2000. Gene expression of osteoprotegerin ligand, osteoprotegerin, and receptor activator of NF-kappaB in giant cell tumor of bone: possible involvement in tumor cell-induced osteoclast-like cell formation. Am. J. Pathol. **156:**761–767.
30. **Iezzi, M., G. Escher, P. Meda, A. Charollais, G. Baldini, F. Darchen, C. B. Wollheim, and R. Regazzi.** 1999. Subcellular distribution and function of Rab3A, B, C, and D isoforms in insulin-secreting cells. Mol. Endocrinol. **13:**202–212.
31. **Jahn, R.** 2004. Principles of Exocytosis and Membrane Fusion. Ann. N. Y. Acad. Sci. **1014:**170–178.
32. **Jahn, R., and T. C. Sudhof.** 1999. Membrane fusion and exocytosis. Annu. Rev. Biochem. **68:**863–911.
33. **Johnston, P. A., B. T. Archer, 3rd, K. Robinson, G. A. Mignery, R. Jahn, and T. C. Sudhof.** 1991. rab3A attachment to the synaptic vesicle membrane mediated by a conserved polyisoprenylated carboxy-terminal sequence. Neuron **7:**101–109.
34. **Jones, S., R. J. Litt, C. J. Richardson, and N. Segev.** 1995. Requirement of nucleotide exchange factor for Ypt1 GTPase mediated protein transport. J. Cell Biol. **130:**1051–1061.
35. **Kaifu, T., J. Nakahara, M. Inui, K. Mishima, T. Momiyama, M. Kaji, A. Sugahara, H. Koito, A. Ujike-Asai, A. Nakamura, K. Kanazawa, K. Tan-Takeuchi, K. Iwasaki, W. M. Yokoyama, A. Kudo, M. Fujiwara, H. Asou, and T. Takai.** 2003. Osteopetrosis and thalamic hypomyelinosis with synaptic degeneration in DAP12-deficient mice. J. Clin. Investig. **111:**323–332.
36. **Knop, M., E. Aareskjold, G. Bode, and V. Gerke.** 2004. Rab3D and annexin A2 play a role in regulated secretion of vWF, but not tPA, from endothelial cells. EMBO J. **23:**2982–2992.
37. **Lam, J., S. Takeshita, J. E. Barker, O. Kanagawa, F. P. Ross, and S. L. Teitelbaum.** 2000. TNF-alpha induces osteoclastogenesis by direct stimulation of macrophages exposed to permissive levels of RANK ligand. J. Clin. Investig. **106:**1481–1488.
38. **Lledo, P. M., L. Johannes, P. Vernier, R. Zorec, F. Darchen, J. D. Vincent, J. P. Henry, and W. T. Mason.** 1994. Rab3 proteins: key players in the control of exocytosis. Trends Neurosci. **17:**426–432.
39. **Lledo, P. M., P. Vernier, J. D. Vincent, W. T. Mason, and R. Zorec.** 1993. Inhibition of Rab3B expression attenuates Ca(2+)-dependent exocytosis in rat anterior pituitary cells. Nature **364:**540–544.
40. **Luzio, J. P., B. Brake, G. Banting, K. E. Howell, P. Braghetta, and K. K. Stanley.** 1990. Identification, sequencing and expression of an integral membrane protein of the trans-Golgi network (TGN38). Biochem. J. **270:**97–102.
41. **Martelli, A. M., G. Baldini, G. Tabellini, D. Koticha, and R. Bareggi.** 2000. Rab3A and Rab3D control the total granule number and the fraction of granules docked at the plasma membrane in PC12 cells. Traffic **1:**976–986.
42. **Martelli, A. M., R. Bareggi, G. Baldini, P. E. Scherer, and H. F. Lodish.** 1995. Diffuse vesicular distribution of Rab3D in the polarized neuroendocrine cell line AtT-20. FEBS Lett. **368:**271–275.
43. **Marzesco, A. M., I. Dunia, R. Pandjaitan, M. Recouvreur, D. Dauzonne, E. L. Benedetti, D. Louvard, and A. Zahraoui.** 2002. The small GTPase Rab13 regulates assembly of functional tight junctions in epithelial cells. Mol. Biol. Cell **13:**1819–1831.
44. **McHugh, K. P., K. Hodivala-Dilke, M. H. Zheng, N. Namba, J. Lam, D. Novack, X. Feng, F. P. Ross, R. O. Hynes, and S. L. Teitelbaum.** 2000. Mice lacking beta3 integrins are osteosclerotic because of dysfunctional osteoclasts. J. Clin. Investig. **105:**433–440.
45. **Millar, A. L., N. J. Pavios, J. Xu, and M. H. Zheng.** 2002. Rab3D: a regulator of exocytosis in non-neuronal cells. Histol. Histopathol. **17:**929–936.
46. **Mulari, M., J. Vaaraniemi, and H. K. Vaananen.** 2003. Intracellular membrane trafficking in bone resorbing osteoclasts. Microsc. Res. Tech. **61:**496–503.
47. **Mulari, M. T., H. Zhao, P. T. Lakkakorpi, and H. K. Vaananen.** 2003. Osteoclast ruffled border has distinct subdomains for secretion and degraded matrix uptake. Traffic **4:**113–125.
48. **Nesbitt, S. A., and M. A. Horton.** 1997. Trafficking of matrix collagens through bone-resorbing osteoclasts. Science **276:**266–269.
49. **Nguyen, D., A. Jones, G. K. Ojakian, and R. D. Raffaniello.** 2003. Rab3D redistribution and function in rat parotid acini. J. Cell. Physiol. **197:**400–408.
50. **Nishio, H., T. Suda, K. Sawada, T. Miyamoto, T. Koike, and Y. Yamaguchi.** 1999. Molecular cloning of cDNA encoding human Rab3D whose expression is upregulated with myeloid differentiation. Biochim. Biophys. Acta **1444:**283–290.
51. **Nonet, M. L., J. E. Staunton, M. P. Kilgard, T. Fergestad, E. Hartwieg, H. R. Horvitz, E. M. Jorgensen, and B. J. Meyer.** 1997. Caenorhabditis elegans rab-3 mutant synapses exhibit impaired function and are partially depleted of vesicles. J. Neurosci. **17:**8061–8073.
52. **Novack, D. V., L. Yin, A. Hagen-Stapleton, R. D. Schreiber, D. V. Goeddel, F. P. Ross, and S. L. Teitelbaum.** 2003. The IkappaB function of NF-kappaB2 p100 controls stimulated osteoclastogenesis. J. Exp. Med. **198:**771–781.
53. **Ohnishi, H., L. C. Samuelson, D. I. Yule, S. A. Ernst, and J. A. Williams.** 1997. Overexpression of Rab3D enhances regulated amylase secretion from pancreatic acini of transgenic mice. J. Clin. Investig. **100:**3044–3052.
54. **Parfitt, A. M., M. K. Drezner, F. H. Glorieux, J. A. Kanis, H. Malluche, P. J. Meunier, S. M. Ott, and R. R. Recker.** 1987. Bone histomorphometry: standardization of nomenclature, symbols, and units. Report of the ASBMR Histomorphometry Nomenclature Committee. J. Bone Miner. Res. **2:**595–610.
55. **Pavlos, N. J., J. Xu, J. M. Papadimitriou, and M. H. Zheng.** 2001. Molecular cloning of the mouse homologue of Rab3c. J. Mol. Endocrinol. **27:**117–122.
56. **Pfeffer, S., and D. Aivazian.** 2004. Targeting Rab GTPases to distinct membrane compartments. Nat. Rev. Mol. Cell Biol. **5:**886–896.
57. **Pfeffer, S. R.** 2001. Rab GTPases: specifying and deciphering organelle identity and function. Trends Cell Biol. **11:**487–491.
58. **Raffaniello, R. D., J. Lin, R. Schwimmer, and G. K. Ojakian.** 1999. Expression and localization of Rab3D in rat parotid gland. Biochim. Biophys. Acta **1450:**352–363.

59. **Riedel, D., W. Antonin, R. Fernandez-Chacon, G. Alvarez de Toledo, T. Jo, M. Geppert, J. A. Valentijn, K. Valentijn, J. D. Jamieson, T. C. Sudhof, and R. Jahn.** 2002. Rab3D is not required for exocrine exocytosis but for maintenance of normally sized secretory granules. Mol. Cell. Biol. **22:**6487–6497.
60. **Roa, M., F. Paumet, J. Le Mao, B. David, and U. Blank.** 1997. Involvement of the ras-like GTPase rab3d in RBL-2H3 mast cell exocytosis following stimulation via high affinity IgE receptors (Fc epsilonRI). J. Immunol. **159:** 2815–2823.
61. **Salo, J., P. Lehenkari, M. Mulari, K. Metsikko, and H. K. Vaananen.** 1997. Removal of osteoclast bone resorption products by transcytosis. Science **276:** 270–273.
62. **Saltel, F., O. Destaing, F. Bard, D. Eichert, and P. Jurdic.** 2004. Apatite-mediated actin dynamics in resorbing osteoclasts. Mol. Biol. Cell **15:**5231–5241.
63. **Schluter, O. M., M. Khvotchev, R. Jahn, and T. C. Sudhof.** 2002. Localization Versus Function of Rab3 Proteins. Evidence for a common regulatory role in controlling fusion. J. Biol. Chem. **277:**40919–40929.
64. **Schluter, O. M., F. Schmitz, R. Jahn, C. Rosenmund, and T. C. Sudhof.** 2004. A complete genetic analysis of neuronal Rab3 function. J. Neurosci. **24:** 6629–6637.
65. **Schmitt, H. D., P. Wagner, E. Pfaff, and D. Gallwitz.** 1986. The ras-related YPT1 gene product in yeast: a GTP-binding protein that might be involved in microtubule organization. Cell **47:**401–412.
66. **Seabra, M. C.** 1998. Membrane association and targeting of prenylated Ras-like GTPases. Cell Signal. **10:**167–172.
67. **Stacey, K. J., I. L. Ross, and D. A. Hume.** 1993. Electroporation and DNA-dependent cell death in murine macrophages. Immunol Cell Biol **71:**75–85.
68. **Stenbeck, G.** 2002. Formation and function of the ruffled border in osteoclasts. Semin. Cell. Dev. Biol. **13:**285–292.
69. **Stenbeck, G., and M. A. Horton.** 2004. Endocytic trafficking in actively resorbing osteoclasts. J. Cell Sci. **117:**827–836.
70. **Suda, T., N. Takahashi, and T. J. Martin.** 1992. Modulation of osteoclast differentiation. Endocr. Rev. **13:**66–80.
71. **Teitelbaum, S. L.** 2000. Bone resorption by osteoclasts. Science **289:**1504–1508.
72. **Tooze, S. A., G. J. Martens, and W. B. Huttner.** 2001. Secretory granule biogenesis: rafting to the SNARE. Trends Cell Biol. **11:**116–122.
73. **Tuvim, M. J., R. Adachi, J. F. Chocano, R. H. Moore, R. M. Lampert, E. Zera, E. Romero, B. J. Knoll, and B. F. Dickey.** 1999. Rab3D, a small GTPase, is localized on mast cell secretory granules and translocates to the plasma membrane upon exocytosis. Am. J. Respir. Cell Mol. Biol. **20:**79–89.
74. **Vaananen, H. K., H. Zhao, M. Mulari, and J. M. Halleen.** 2000. The cell biology of osteoclast function. J. Cell Sci. **113:**377–381.
75. **Vaaraniemi, J., J. M. Halleen, K. Kaarlonen, H. Ylipahkala, S. L. Alatalo, G. Andersson, H. Kaija, P. Vihko, and H. K. Vaananen.** 2004. Intracellular machinery for matrix degradation in bone-resorbing osteoclasts. J. Bone Miner. Res. **19:**1432–1440.
76. **Valentijn, J. A., D. Sengupta, F. D. Gumkowski, L. H. Tang, E. M. Konieczko, and J. D. Jamieson.** 1996. Rab3D localizes to secretory granules in rat pancreatic acinar cells. Eur. J. Cell Biol. **70:**33–41.
77. **Walter, M., S. G. Clark, and A. D. Levinson.** 1986. The oncogenic activation of human p21ras by a novel mechanism. Science **233:**649–652.
78. **Weber, E., G. Berta, A. Tousson, P. St John, M. W. Green, U. Gopalokrishnan, T. Jilling, E. J. Sorscher, T. S. Elton, D. R. Abrahamson, and et al.** 1994. Expression and polarized targeting of a rab3 isoform in epithelial cells. J. Cell Biol. **125:**583–594.
79. **Xu, J., J. W. Tan, L. Huang, X. H. Gao, R. Laird, D. Liu, S. Wysocki, and M. H. Zheng.** 2000. Cloning, sequencing, and functional characterization of the rat homologue of receptor activator of NF-kappaB ligand. J. Bone Miner. Res. **15:**2178–2186.
80. **Zerial, M., and H. McBride.** 2001. Rab proteins as membrane organizers. Nat. Rev. Mol. Cell Biol. **2:**107–117.
81. **Zhao, H., T. Laitala-Leinonen, V. Parikka, and H. K. Vaananen.** 2001. Downregulation of small GTPase Rab7 impairs osteoclast polarization and bone resorption. J. Biol. Chem. **276:**39295–39302.
82. **Zheng, M. H., Y. Fan, S. Wysocki, D. J. Wood, and J. M. Papadimitriou.** 1993. Detection of mRNA for carbonic anhydrase II in human osteoclast-like cells by in situ hybridization. J. Bone Miner. Res. **8:**113–118.